Three-dimensional structure of *Vp*, *Vs* and *Vp/Vs* in the upper crust of the Marmara region, NW Turkey

Şerif Bariş[1]*, Junichi Nakajima[2], Akira Hasegawa[2], Yoshimori Honkura[1], Akihiko Ito[3], and S. Balamir Üçer[4]

[1]*Department of Earth and Planetary Sciences, Tokyo Institute of Technology, Tokyo, Japan*
[2]*Research Center for Prediction of Earthquakes and Volcanic Eruptions, Tohoku University, Sendai, Japan*
[3]*Faculty of Education, Utsunomiya University, Utsunomiya, Japan*
[4]*Department of Geophysics, Kandilli Observatory and Earthquake Research Institute, Boğaziçi University, Istanbul, Turkey*

We applied a 3-D seismic tomography inversion algorithm to arrival-time data obtained, during 18 years from 1985 to 2002, from local seismic networks and aftershock studies in the Marmara region, in order to better understand the upper crustal structure of the complex tectonic region. We integrated all the available data set into a common data set and relocated the events, using a 1-D velocity model. We then selected 3,949 earthquakes and obtained 92355 arrival times, in total, consisting of 59,313 *P*-wave and 33,042 *S*-wave arrival times. In this paper we present detailed crustal structures for Vp, Vs and Vp/Vs ratios from the surface down to 15 km depth with good resolution in terms of the hit count analysis of seismic rays, the checkerboard and restoring resolution tests for the studied region. The results obtained from the inversion suggest that the western part of the North Anatolian Fault Zone shows strong lateral heterogeneity. We concluded that no clear pattern exists between the distribution of microearthquakes and aftershocks and the velocity perturbations presented in this paper. This is probably due to complex tectonic and geological structures. Large coseismic slip associated with the two recent strong earthquakes was found to correspond to higher velocity anomalies, as was often found recently. On the other hand, low velocity values correspond to the sedimentary units or the alluvium regions, as supported by the low resistivity and gravity values. Thus the results presented in this paper are quite consistent with the other data such as gravity, resistivity and magnetic anomalies, indicating that our model is reliable and efficient and it should be useful for further interpretation of tectonic and geological problems in this region. It should be pointed out, however, that the results of *S*-wave perturbations and Vp/Vs ratio could not be discussed in detail because of insufficient quality of the *S*-wave data and the reliability of the results is not very high. Nonetheless, the fact that recent large Izmit earthquake and moderate aftershocks that occurred in or around the high velocity zones near the low velocity region suggests that high velocity regions found in the area close to Istanbul in the Marmara Sea and also at the Iznik-Mekece fault are potential sites for strain energy accumulation and release.

Key words: Marmara Sea, North Anatolian Fault Zone, seismic tomography, seismic velocity structure, seismicity.

1. Introduction

The Anatolian block is located in the highly active Alpine-Himalayan seismic belt and characterized by the collision of the Arabian and the African plates with the Eurasian plate (McKenzie, 1972), as shown in Fig. 1. The collision probably started during Early Miocene (Yilmaz *et al.*, 1995) and gave rise to shortening, thickening and uplift of the Anatolian block. The Anatolian block began to move west, along the North Anatolian Fault Zone (NAFZ), during Late Miocene to Pliocene about 5.7 million years ago (Barka, 1992). Yaltirak *et al.* (2000) suggested, however, that the NAFZ started its activity later than 3.7 million years. The rate of the lateral displacement along the NAFZ has been estimated from regional seismotectonic (Canitez

and Üçer, 1967; Eyidoğan *et al.*, 1998; Taymaz *et al.*, 1991) and geodetic (Reilinger *et al.*, 1997; McClusky *et al.*, 2000) slip-rate measurements, ranging from 17 to 24 mm/year in the E-W direction in the Marmara Sea region, near the western end of NAFZ. The geologically estimated total displacement is about 1 km since Quaternary and several tens of kilometers since Pliocene.

The NAFZ is in fact regarded as a large-scale transform fault like the San Andreas Fault (Barka, 1992), and has been the sites of numerous disastrous earthquakes including the Erzincan earthquake of 1939 (Mw7.9), the Izmit (Mw7.4) and the Duzce (Mw7.2) earthquakes of 1999. It is a nearly 1500 km long dextral strike-slip fault extending from Karliova triple junction in the east (Eastern Turkey), crossing through the Marmara Sea and entering the North Aegean Sea and mainland Greece in the west. The Marmara region in the western part of the NAFZ, defined in this paper as the region between Bolu and the Dardanelles, is a transition zone between the strike-slip regime in the east and the extension regime in the west, the Aegean Sea.

*Present address: Department of Geophysics, Faculty of Engineering, University of Kocaeli, Veziroğlu Campus, Kocaeli, Turkey.
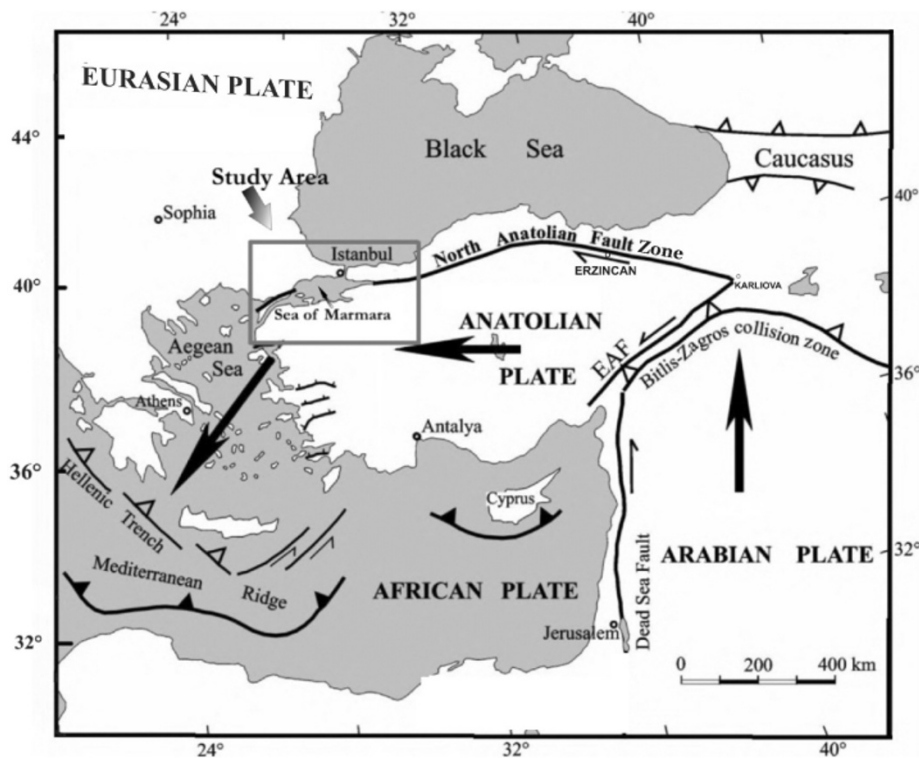
Fig. 1. Location of the investigated region (rectangular area) shown together with the active tectonic map of the Anatolian plate and the surrounding regions. Lines with solid triangles represent the active subduction zones, lines with open triangles the active trust faults, and solid lines the strike-slip faults. Plate motions are shown by large solid arrows. EAF stands for the East Anatolian Fault (after Okay *et al*., 2000).

In fact, the Marmara region has shown complex tectonic features with high seismic activity (Barka and Kandinsky-Cade, 1988). In particular, the NAFZ zone splays into two main branches around Bolu (32°E in longitudes), and then into three branches around Geyve-Adapazari (30°E). The three branches have been called the northern (Sapanca Lake, the Gulf of Izmit, the northern Marmara Sea, Murefte, the Gulf of Saros), the middle (Geyve, the south of Iznik Lake, the west of Gemlik Bay, Bandirma, Ezine) and the southern (Geyve, Edremit) branches (Dewey and Şengör, 1979; Şengör *et al*., 1985). Smith *et al*. (1995) and Okay *et al*. (1999) proposed that the NAFZ would be further separated into more branches in the Marmara Sea. Names of geographical locations and cities are given in Figs. 1 and 4(a).

Historical seismicity and recent GPS studies indicate that the northern branch has been more active, followed by the southern branch and then by the central one (Ambraseys and Finkel, 1991, 1995; Oral *et al*., 1995; Barka and Reilinger, 1997; Barka, 1999; Ayhan *et al*., 2002; Finkel, 2002). In addition, recent detailed micro-earthquake studies show that the seismicity has been most active along the northern branch (Üçer *et al*., 1997; Bariş *et al*., 2002). Current seismic risk in the Marmara Sea region is extremely high, in particular for several large cities with total population of about 20 million (Bursa, Tekirdağ, Izmit, Yalova, Edirne, Balikesir, Canakkale and Istanbul). For example, Istanbul is a rapidly growing metropolis that has been heavily damaged by the earthquakes which had occurred in the Marmara Sea region twelve times during the past 15 centuries (Genç and Mazak, 2001); the 1894 earthquake with

the estimated moment magnitude of 7.0 was the last historical earthquake. The west of the Izmit earthquake rupture zone has remained as an unruptured fault segment of nearly 160 km. According to Parson *et al*. (2000), the probability of large earthquake occurrence in the Marmara Sea is as high as 62±15% within 30 years and 32±12% during the next decade.

In view of such high seismic risk, various kinds of studies have been undertaken in the Marmara region. Detailed investigations of geology and tectonics of the Marmara Sea and its surrounding regions have been made (Şengör *et al*., 1985; Yilmaz *et al*., 1995; Üçer *et al*., 1997; Gürbüz *et al*., 2000; Yaltirak, 2002). GPS measurements have been conducted to estimate the relative rates of displacement of the Anatolian Block with respect to Eurasia (Starub and Kahle, 1994, 1997; Oral *et al*., 1995; Barka and Reilinger, 1997; Ayhan *et al*., 2002). Marine seismic experiments have been carried out across the pull-apart basins and the active fault traces beneath the Marmara Sea to obtain detailed information on shallow fault structures and fault movements (Smith *et al*., 1995; Okay *et al*., 1999; Demirbağ *et al*., 2003). Neotectonic and paleoseismological studies on several segments of the NAFZ provided new quantitative information about the tectonic process and the time record of major earthquakes (Ikeda *et al*., 1989; Barka, 1992). Some other geophysical observations such as gravity, magnetotellurics (MT) and the magnetic field have also been undertaken (Honkura *et al*., 1985; Işikara *et al*., 1985; Tunçer *et al*., 1991a, b; Honkura and Işikara, 1991; Gürer, 1996; Honkura *et al*., 2000; Adatepe *et al*., 2002; Tank *et al*., 2003; Ateş *et al*., 2003).

Table 1. Available data from various networks. Number of seismic stations is for those belonging to the study area.

Name of the network	Operation period	Number of seismic stations	Number of events	Type of observation
MARNET	1976–Present	20	15000	Permanent
IZINET	1993–Present	15	4500	Permanent
ISTNET	August 2002–Present	6	100	Permanent
DAT Stations	August 1999–February 2000	10	6000	Aftershock-Temporary
EDR Stations	August 1999–March 2000	10	7000	Aftershock-Temporary
LAMONT Stations	August 1999–February 2000	83	15000	Aftershock-Temporary
Seismicity of Bursa	October 1996–June 1997	12	3700	Project-Temporary
Seismicity of Marmara	September–November 1998	30	200	Project-Temporary
TUBITAK	August–December 1999	62	500	Project-Temporary

Most of these studies are directed toward the understanding of shallow structures associated with active faults rather than the seismogenic zones which are supposed to be located between 7 and 15 km in depth, and hence the information on the deeper structure is still insufficient. Also, important information such as the earthquake generation process coupled with heterogeneity of the structure is not available. In this respect, 3-D seismic tomography studies can contribute to better understanding of heterogeneous structures in the seismogenic zone. This is the reason why we took up the present study of 3-D tomography in the Marmara region.

Microearthquake activity in this region has been monitored continuously since the MARNET seismic network was established in 1976 (Üçer *et al.*, 1985). Because of insufficient network coverage, however, the distributions of earthquakes and seismic stations in and around Marmara region have not been good enough for a study of 3-D velocity structure. In the meantime, tomography studies were performed by Kuleli *et al.* (1995) and by Nakamura *et al.* (2002) for some parts of the Marmara region. In particular, Kuleli *et al.* (1995) attempted a tomography of *P*-wave velocity for the deeper structure of the Aegean Sea region including the western part of the Marmara Sea, whereas Nakamura *et al.* (2002) evaluated *P*-wave structure of the aftershock area of the 1999 Izmit earthquake. However, their data sets are limited and both the grid size and the resolution were rather poor.

After the IZINET seismic network were established in 1993 in the eastern part of the Marmara region, we could collect a large amount of aftershock data from the Izmit and the Duzce earthquakes in 1999. Hence the data set should now be good enough to perform a study of three-dimensional velocity structure of better resolution. In fact, we combined all the available seismic arrival-time data from some permanent seismic networks such as MARNET and IZINET, and also from aftershock observations after the Izmit and the Duzce earthquakes. We also incorporated the results from the past projects on seismicity in the Marmara region. We now apply a tomography method to estimate 3-D Vp, Vs and Vp/Vs structures beneath the Marmara region. Then we will try to interpret the obtained velocity images in terms of material properties, rock types, fluid distribution, and so on. It would also be useful to compare the results with other geophysical information such as gravity and the resistivity.

2.   Data and Method

We first attempted to combine all the seismic phase arrival data which are available for the study area from the existing networks and also from various studies for the period from 1985 to 2002. Seismicity of the Marmara region has mainly been monitored by the National Earthquake Monitoring Center (NEMC), Kandilli Observatory and Earthquake Research Institute of Boğaziçi University (BUKOERI), with the MARNET seismic network since its installation in 1976 (Üçer *et al.*, 1985) and some other national seismic network stations. The MARNET network consists of nine single-component radio-telemetry stations surrounding the Marmara Sea and has been operated by the NEMC. This network was the first modern seismological network in Turkey and only this network has provided continuous seismic information for the Marmara region since its installation. Hereafter the seismic stations belonging to MARNET and the national seismic network are referred to as KOERI. Another network called IZINET was installed in the eastern part of the Marmara region in August 1992 with six seismic stations, in order to monitor the microearthquake activity and provide the data of high quality in this region (Ito *et al.*, 1994; Bariş *et al.*, 1996a, b; Bariş *et al.*, 2002; Ito *et al.*, 2000, 2002). It was installed in the east of MARNET in view of increasing earthquake risk in the western part of the NAFZ (Toksöz *et al.*, 1979). The number of seismic stations increased to 16 in 1998. Now the present networks cover all three branches of the NAFZ. In August 2002, the ISTNET network consisting of six 3-component seismometers was installed in and around Istanbul and started to record seismic events in the northern and northwestern parts of Istanbul.

The initial data set used for relocations of hypocenters was enriched by adding aftershock and temporary observation results. The details of station distribution, observation system and information for the data provided by aftershock and seismicity projects are shown in Sellami *et al.* (1997), Eyidoğan *et al.* (1998), Seeber *et al.* (2000), Gürbüz *et al.* (2000), Nakamura *et al.* (2002) and Iio *et al.* (2002). We used routine picks by several different observers and merged data from different networks to make initial data set for hypocenter locations. In Table 1, we briefly summarized some descriptions of each network such as the recording period, the number of seismic stations and so on. In total, 53,000 earthquakes including aftershocks of the Izmit and the Duzce earthquakes during recent 18 years were relocated with the revised version of HYPO71PC (Lee and
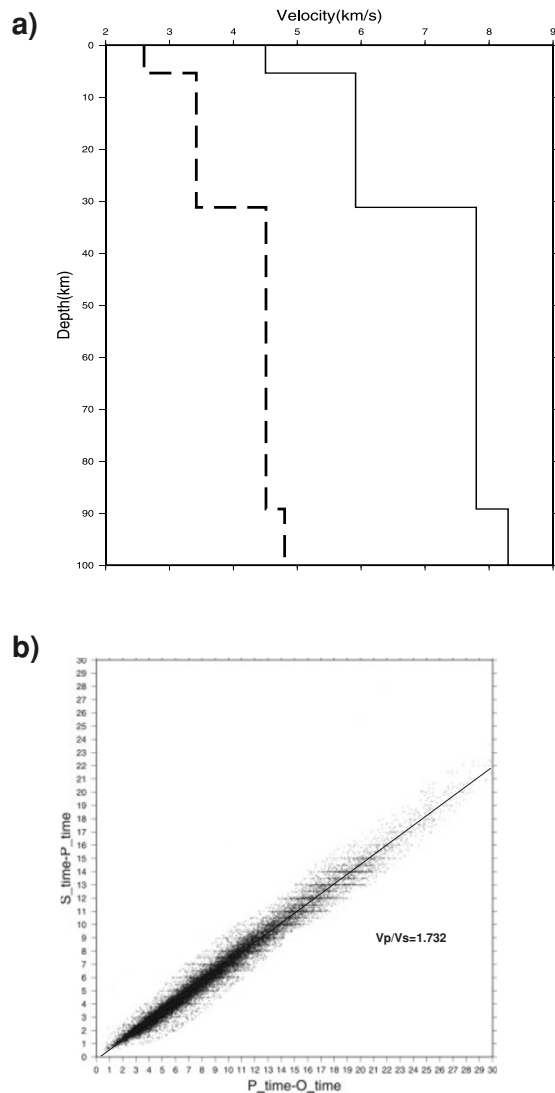
a)

b)

Fig. 2. (a) The minimum 1-D model used in the routine location of earthquakes (Üçer, 2002, personal communication) and also used as an initial model for the 3-D tomograpic inversion. The solid line represents the *P*-wave velocity and the dashed line the *S*-wave velocity. (b) The modified Wadati diagram showing *P* arrival-time minus origin time vs *S* arrival-time minus *P* arrival-time, and the least squares best fitted Vp/Vs ratio of 1.732 for the best quality data.

Lahr, 1975; Lee and Valdes, 1985); here, more than local and regional 325 stations were used for initial relocation in whole Turkey. This program has been routinely used at the NEMC of BUKOERI.

We used *P*- and *S*-wave reading for relocations and the magnitudes were calculated by applying the duration-dependent formula, which has been widely used for local earthquakes at KOERI. For aftershocks, however, magnitudes were not determined during preparation of the manuscript. We used the 1-D initial velocity model shown in Fig. 2(a) and selected 1.0 and 0.5 as weights for *P* and *S* waves for relocations. We also used the *S*-wave velocity for hypocenter relocations, assuming $Vp/Vs = 1.73$ as generally used by KOERI for routine locations of local seismic events in the western part of Turkey. To verify this assumption on the Vp/Vs ratio, we applied the Wadati method, and the modified Wadati diagram yields $Vp/Vs = 1.732$,

as shown in Fig. 2(b), which is in good agreement with the reference value used for locations of earthquakes. After re-locations we omitted the bad quality data from the data set. If the standard error of epicenter and depth is greater than or equal to 5 km, or the number of phase reading is less than 10 (original value was 6 in the computer programme), or the gap is greater than 180° or the rms-value is greater than or equal to 0.5 seconds, or the epicentral distance in km to the nearest station is greater than 50 km, hypocenter solutions are assigned as bad quality data, as described in detail in the manual of HYPO71PC (Lee and Lahr, 1975). If one of the above criteria is met in our relocated events, we removed such events from the initial data set for using tomographic inversion, and we have only 33,352 events remained, as plotted in Fig. 3(a).

Figure 3 shows the locations of all the seismic stations that we used for relocations of seismic events. The stations are densely and uniformly distributed in the eastern and central parts of the study area. Unfortunately, however, the station coverage is not good in the western, northwestern and southeastern parts of the region.

In order to select the best set of seismic events for the inversion, we divided the study region into 120,000 blocks with spatial size of about $10 \times 10 \times 0.5$ km^3 between 0 and 50 km depth. The event selection criteria are mainly based on the condition that the ray should pass through at least one block. As a result, we selected 3,949 earthquakes as given in Fig. 3(b). They were used for tomographic inversion and also for relocations with the new velocity model obtained by the inversion. The total number of *P*-arrivals from 3,949 earthquakes is 59,313, whereas for *S*-arrivals it is 33,042. In total, 248 local seismic stations, installed permanently or temporally in the study region were used for the data during 1985 to 2002. In order to avoid the effect of Pn velocity anisotropy and the Moho depth variation, we used only the arrival times with epicentral distances shorter than 200 km. Picking accuracy for the aftershock data and the IZINET network is better than KOERI readings for *P* and *S* waves. In fact, most of the permanent seismic stations have only a single component, whereas all the temporary seismic stations for aftershock monitoring were equipped with 3-component seismometers. KOERI stations still rely on paper drum recorders and reading accuracy of arrival time of *P* wave is estimated to be around 0.05–0.2 seconds and 0.1–0.7 seconds for *S* wave. Accuracy of *P* and *S* waves for the other data sets is better than these values. Most of the data used for tomographic inversion are recent aftershock data recorded digitally.

In order to determine the 3-D crustal structure in the Marmara region, we used the tomographic technique developed by Zhao (1991) and improved by Zhao *et al*. (1992). This technique applies ray-tracing by the pseudo-bending method and uses a conjugate gradient solver, the LSQR algorithm of Paige and Saunders (1982), to invert a large amount of the observed arrival times to the unknown parameters. Um and Thurber (1987) tested this algorithm by using different data sets having different travel times. They noted that this ray tracing technique is efficient and can be used for routine earthquake location and for velocity inversion programs in laterally heterogeneous seismic velocity structure.
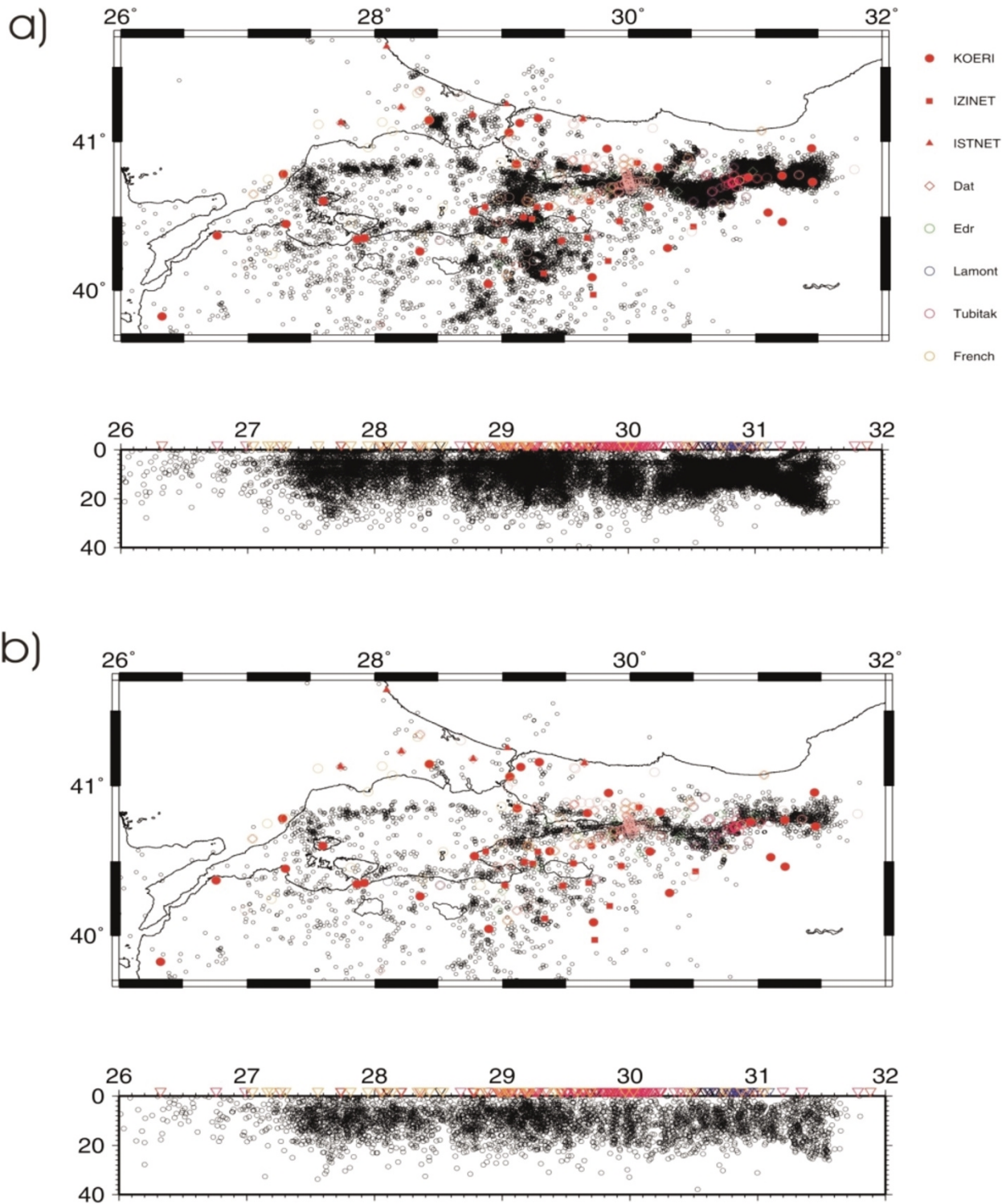
Fig. 3. (a) Relocated 33,532 earthquakes (small open circles) (1985–2002) from the integrated data which were derived from various permanent and temporary networks used as the initial database for selecting earthquakes. (b) 3,949 earthquakes selected to perform 3-D tomographic inversion and the distribution of used stations for inversion. The distribution of seismic stations used for the relocation and inversion is shown with different symbols for the data sources shown in Table 1.

Zhao *et al.* (1992) concluded that the pseudo-bending technique can find an accurate ray path in a fully 3-D form, no matter how long the hypocentral distance is. In this method, any seismic discontinuities can be taken into consideration so that we can deal with complex velocity discontinuities. The velocity model we adopted as given in Fig. 2 is not a continuous model but has a velocity jump, and so we used a velocity model with velocity discontinuities. Nonlinear tomographic problem is solved by iteratively conducting linear inversions. In each step of the iteration, the velocity structure and earthquake source parameters are determined simultaneously. The mathematical formulation and the detailed explanation of the method are given in Aki and Lee (1976), Zhao (1991), and Zhao *et al.* (1992).
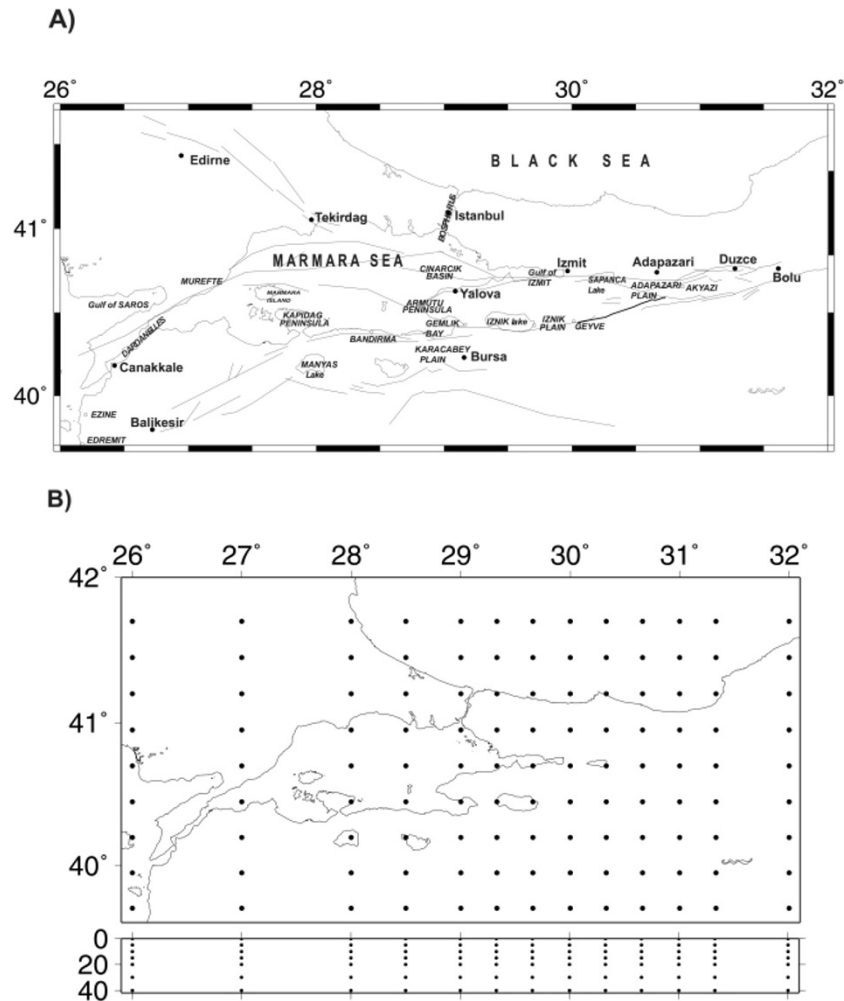
Fig. 4. Plan and E-W cross-sectional views of the variable grid adopted in the inversion.

In this tomographic inversion velocities within each layer are allowed to vary laterally and vertically. A 3-D grid is set up to obtain the 3-D velocity structure. Velocities at each grid node and hypocenter parameters are taken as unknown parameters. The velocity at any point is calculated through linear interpolation of velocities at eight grid nodes surrounding that point. We tried to select the best grid spacing and attempted to use horizontally and vertically variable grid spacing. We could not use the uniform grid spacing, because the ray paths are not uniformly distributed horizontally as well as vertically, and the station distribution is not uniform in the study area. In fact, the grid spacing was chosen so as to have enough ray paths near each grid point.

We first tried to change the grid spacing from a sparse to a denser grid with nodal spacing of 0.40°, 0.33° and 0.25° in the E-W and N-S directions, to perform a resolution test and invert a small amount data set. Subsequently, we selected the best 3-D grid spacing which is shown in Fig. 4. The spacing in the E-W direction was selected as 1° in the westernmost part, between 26°E and 28°E in longitudes. Then it was taken as 0.5° in the area between 28°E and 29°E in longitudes where the station distribution is dense. In the aftershock area of the Izmit and the Duzce earthquakes located east of 29°E, the grid spacing is taken as 0.33°, because of the denser station coverage of this region. In the

N-S direction, the grid spacing is selected equally as 0.25°, starting between 39.7°N and 41.7°N in latitudes. Also after we tried to apply different grid spacing as 2, 3, 4 and 5 km to the vertical direction, we finally decided to use 5 km grid nodes for the vertical direction to the depth of 20 km and then 10 km to the depth of 40 km; hence the layers of grid nodes are at depths of 0, 5, 10 15, 20, 30 and 40 km.

Because of the insufficient number of earthquakes and the bad resolution results according to the CRT and RRT tests and hit count results, we will not discuss any velocity perturbation below 15 km depth for the Vp, Vs and Vp/Vs structures. There are many velocity models for locating earthquakes as proposed by some researchers with different methods and data sets for different parts of the Marmara Sea region: Gürbüz *et al.* (1998), Üçer *et al.* (1997), Ergin *et al.* (2000), Bouchon *et al.* (2000), Pektaş (2001), Ito *et al.* (2002), and Horasan *et al.* (2002). We tried to relocate our data set with different velocity models but RMS values turned out to be larger than the velocity model which is used for tomography. We started to perform tomographic inversion by using a simplest and widely used one-dimensional velocity model of BUKOERI, which is routinely used for the location procedure at BUKOERI for local earthquakes in the western part of Turkey. This model has been derived combining different 1-D velocity models obtained by VE-
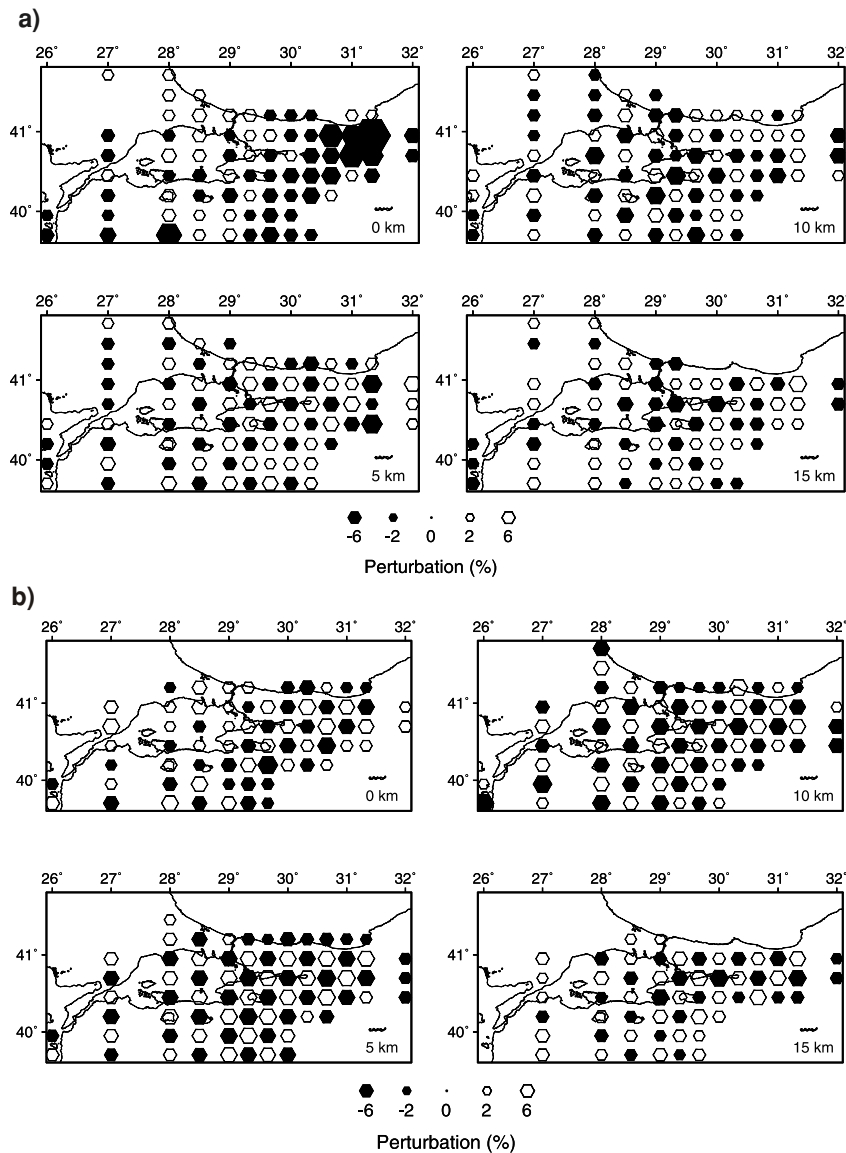
Fig. 5. Results for the checkerboard resolution test for (a) *P* and (b) *S* waves. The depth of each layer is shown in the lower right corner of each map.

LEST (Kissling *et al.*, 1994), quarry blasts and taking into account the seismic refraction profiles for the Marmara region (Bariş *et al.*, 2002; Üçer, 2002, personal communication). This velocity model was already shown in Fig. 2(a).

3. Resolution Tests

3.1 Checkerboard resolution test

In order to assess how adequate the ray coverage would be and also how high the resolution of tomographic inversions would be, we constructed synthetic models and made the so-called checkerboard resolution tests (CRT) with the hit count of ray paths in each grid block. The basic idea of CRT is shown in Humphreys and Clayton (1988) and Inoue *et al.* (1990). We assigned positive and negative velocity perturbation of ±6% alternately to the 3-D grid nodes, and calculated travel times for this model to make the synthetic data. The images of synthetic inversions and hit counts are considered to be useful to examine where the resolution is good or poor. We also added random noises 0.05 s for the *P* wave and 0.1 s for the *S* wave which correspond to pick-

ing errors in the synthetic data. The CRT test is in fact a checkerboard pattern in the 3-D grid.

3.2 Restoring resolution test

The basic idea of restoring resolution test (RRT) is given by Zhao *et al.* (1992). It is believed that the simple CRT test image cannot sufficiently show the resolution for complicated tectonic structures and the RRT test is useful to show the resolution for the study area. In this type of test, the final 3-D velocity model obtained by the inversion is taken as an initial model, and synthetic travel times are then calculated for the model by using the 3-D ray tracing technique. In the RRT test, random noises corresponding to the uncertainty in picking *P*- and *S*-phases of local earthquakes are usually added to the calculated synthetic travel times. By applying the same inversion algorithm to the calculated synthetic data, we obtain the restoring image of the real result.

4. Results

Our present tomographic inversion provides the first reliable 3-D velocity model for the whole Marmara region,
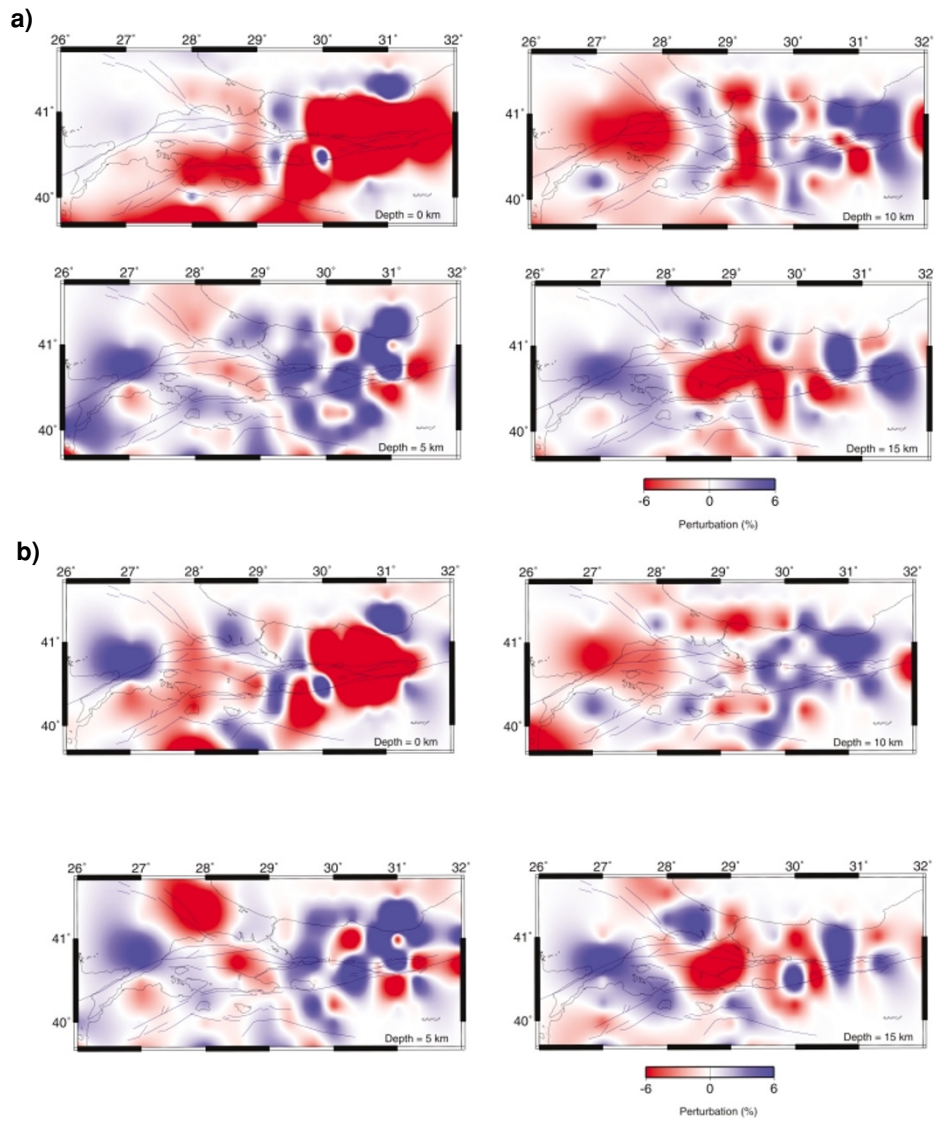
Fig. 6. Results for the restoring resolution test for (a) *P* and (b) *S* waves. The depth of each layer is shown in the lower right corner of each map. Blue and red colors represent high and low velocity perturbations, respectively.
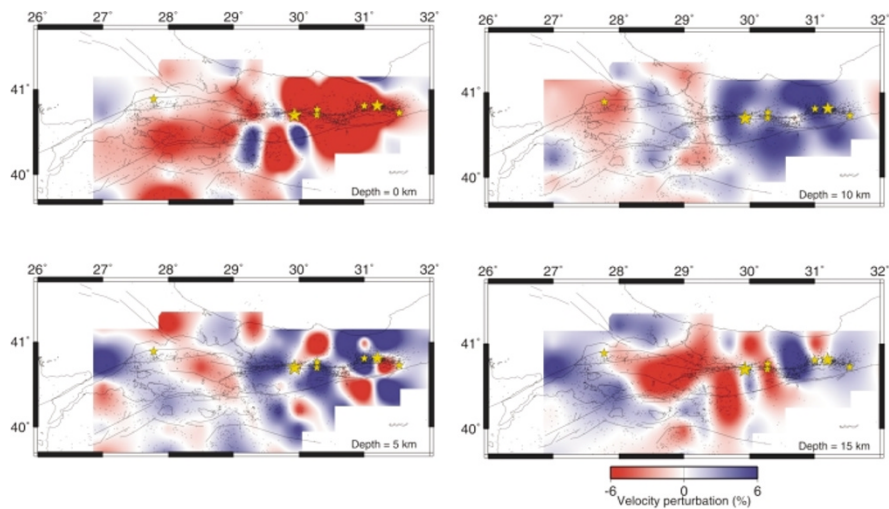

Fig. 7. *P*-wave velocity perturbations obtained by 3-d inversion. The velocity perturbation is defined as the deviation of velocity from the initial velocity given in Fig. 2. Blue and red colors represent high and low velocity perturbations, respectively. Open circles show the epicenters relocated by the inversion. The fault lines are taken from Saroğlu *et al.* (1992), Ikeda and Komut (1999), Okay *et al.* (2000), and Woith (2003). The depth of each layer is given in the lower right corner of each map.

where inhomogeneous, sharp velocity variations have been expected, because of the complex tectonic regime and geology. In this section we explain the results of inversion in detail.

We first tried to obtain the best grid spacing for the horizontal and vertical directions, based on the checkerboard patterns, hit counts and the number of arrival times for each station. As for the vertical direction, the results turned out to be similar for spacing of 5 and 6 km. Only 2, 3 and 4 km depth spacing could not be recovered in our synthetic test and so we decided to use 5 km grid spacing for the depth range from 5 to 20 km. Below 20 km, 10 km grid spacing was selected according to the CRT test and the ray paths.

Evidently, the heterogeneity in the lower crust cannot be examined with the present data set, because most of the earthquakes occurred in the upper crust in the study area. So we focus the tests on the crust to the depth of 15 km. Then we performed the CRT tests for different grid spacing in the horizontal and vertical directions. In Fig. 5, we show a typical checkerboard pattern which seems to ensure good resolution. The hit counts which are not shown here are also large at the locations of high resolution. The results of CRT for the P wave are quite good and the pattern can be recovered at 5, 10 and 15 km depths for most of the study area, as shown in Fig. 5(a). The resolution is relatively low at 15 km depth, because few earthquakes occur at and below this depth. Figure 5(b) shows the resolution for the S wave which is rather poor, compared with the case for the P wave. In particular, the resolution for the S wave is poor below 15 km and hence we cannot discuss on the velocity structure beneath this depth for Vs and Vp/Vs. In general, the checkerboard patterns are well recovered in the regions where the distribution of seismic stations is dense, namely in the central and the eastern parts of the Marmara Sea region. In other regions, the resolution is poor and significant discussion would not be possible, particularly for Vs and Vp/Vs.

The results of restoring resolution test (RRT) are shown in Figs. 6(a) and 6(b) for several layers for Vp and Vs, respectively. In the RRT, the final 3D model is taken as an initial model. Travel times are calculated for the same station and hypocenter pairs as the observation to generate the synthetic data. We added 0.1 s for Vp, 0.4 s for Vs as random noises to the synthetic travel time data. In Figs. 6(a) and 6(b), we show the perturbations in percent from the reference model with blue for faster values and red for slower values for RRT test results. By comparing the RRT images (Figs. 6(a) and (b)) and initial models (Figs. 7 and 8), we can know whether or not and how well the special structures or the main trend in the real result are realistically restored. Comparing images obtained by normal inversion for Vp (Fig. 7) and Vs (Fig. 8) with their RRT images for Vp (Fig. 6(a)) and for Vs (Fig. 6(b)), we can see that the tomographic images by the normal inversion reconstructed for most parts of the study area in the layers for 0–15 km depths. The images located at the edge of the study area are distorted to some extent, as expected. Reconstruction is better for Vp than for Vs, probably due to low quality of S-wave phase readings and less phase arrivals for S waves. We believe that test results can verify the interesting parts

of our results through RRT and CRT results.

Then the inversion was performed with varying grid spacing in the E-W direction and fixed spacing in the N-S direction. Five iterations of simultaneous inversion provided the final results and we also obtained the relocated hypocenters. The average root mean square residuals (rms) for the travel times decreased from 0.159 sec to 0.154 sec for the P wave and 0.161 sec to 0.159 sec for the S wave.

In Figs. 7 and 8, we show the perturbations in percent from the reference model with dark blue for higher velocity and red for lower velocity for Vp and Vs, and light blue for lower values and dark yellow for larger values for Vp/Vs given in Fig. 9. Each figure shows plan views of horizontal layers at different depth slices. Regions without any colors (white) represent poorly resolved areas. In Fig. 7, we clearly see some low and high P-wave velocity regions in the study region. High velocity areas are located in the east of Iznik Lake, in the north of the mainshock of the Izmit earthquake. In the central part of the Marmara Sea, the velocity is not very low in the layers except for top two layers where low velocity regions are dominant. These low velocity zones again prevail at the depth slice of 15 km, covering wider areas.

Lower velocity regions are predominant mainly in thick sedimentary layers or alluvium regions and Pliocene deposits such as the Iznik plain, the Adapazari plain, the Karacabey plain, the Çinarcik basin in the Marmara Sea. Higher velocity regions are mainly located in the higher elevation areas and the metamorphic sequences or the ophiolitic melange series. Lower velocity anomalies are likely to represent high porosity, fracturing, high water or fluid content, high temperature or the quartz amount in the lithology content.

As seen in Fig. 8, the pattern for the S wave is different from that for the P wave. The main difference may probably be due to the fact that the S wave has the resolution different from the P wave and is more sensitive to liquid, high temperature and silicate minerals. It should be noted, however, that the estimation of S-wave velocities is less accurate than that for P wave velocities, because of rather poor S phase readings and the lack of the data even at some important seismic stations. For example, most of the KOERI and IZINET stations are equipped with the single component only and reading of S-wave phases from the vertical seismometers leads to some misinterpretation in arrival time, as observed by Eberhart-Phillips and Michael (1993). On the other hand, we believe that S phase readings are of good quality for the eastern part of the Marmara Sea region; especially in the aftershock area, all the aftershock seismic stations were equipped with three-component seismometers and the digital records of 100 Hz and 2000 Hz sampling frequency are available for 10 EDR stations. In addition, almost all the seismic stations are located on the rock sites.

In most of the study region, we found many areas of higher S-wave velocity at all depth slices. On the other hand, several low S-wave velocity areas are located in the eastern and southern part of the mainshock of the Duzce earthquake, in the east and south of Iznik Lake and in the Armutlu peninsula, around Bosphorus. Also, the lower S-wave perturbations are seen at the sedimentary layer in
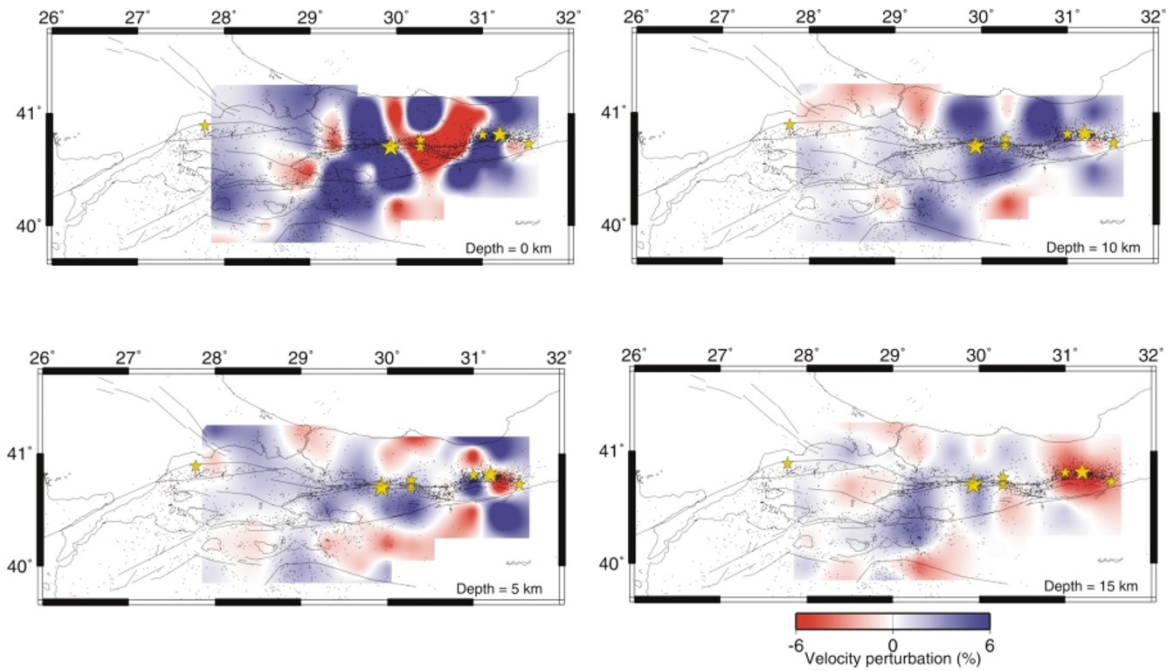
Fig. 8. *S*-wave velocity perturbations obtained by the inversion. The velocity perturbation is defined as the deviation of velocity from the initial velocity given in Fig. 2. Blue and red colors represent high and low velocity perturbations, respectively. Open circles show the epicenters relocated by the inversion. The fault lines are taken from Saroğlu *et al.* (1992), Ikeda and Komut (1999), Okay *et al.* (2000), and Woith (2003). The depth of each layer is given in the lower right corner of each map.
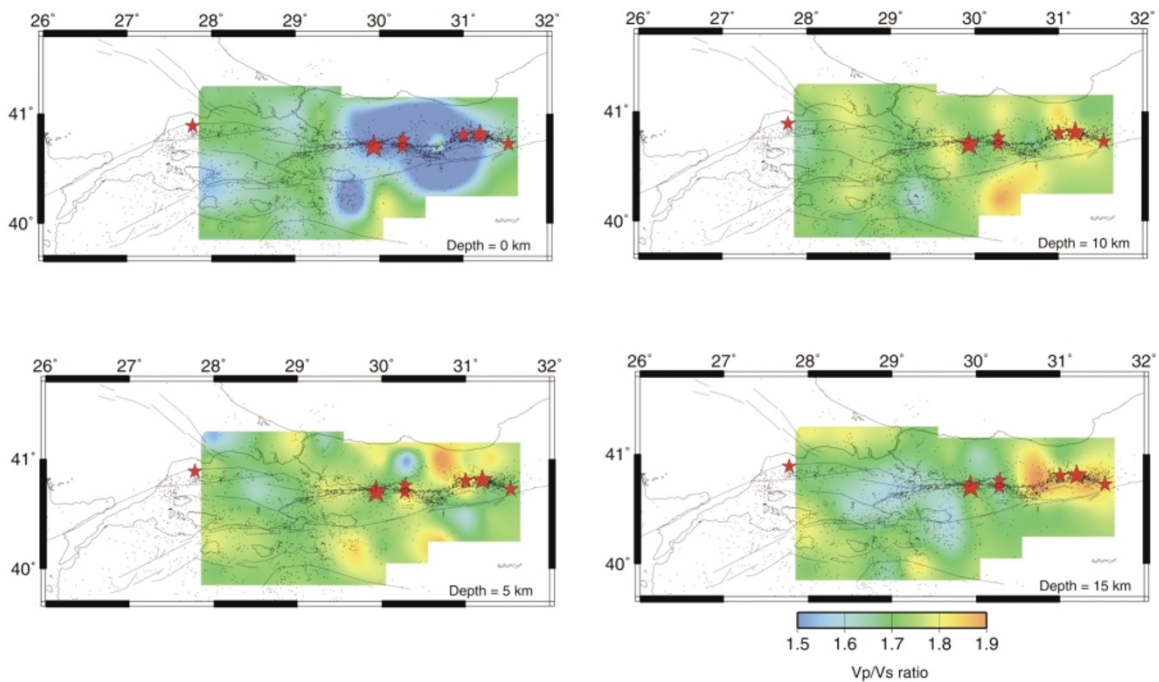

Fig. 9. *Vp/Vs* values obtained by the inversion. Yellow and blue colors represent high and low *Vp/Vs*, respectively. Open circles show the epicenters relocated by the inversion. The fault lines are taken from Saroğlu *et al.* (1992), Ikeda and Komut (1999), Okay *et al.* (2000), and Woith (2003). The depth of each layer is given in the lower right corner of each map.

the Çinarcik basin as well as the Holocene alluvium plains situated at Izmit, Akyazi, Duzce and surrounding regions. Such characteristics imply that some low *P*-wave velocity areas might not be due to high fluid contents.

In Fig. 9, we show the results for *Vp/Vs*. Most of the areas show normal or higher values of *Vp/Vs*. In the eastern part located between the Izmit and Duzce mainshock areas,

low values of *Vp/Vs* prevail in the top layer, but the spatial extent of this low *Vp/Vs* zone is reduced and it disappears in the 2nd layer. We also see the low values in the second layer at the eastern part of Çinarcik Basin, south of Akyazi and northeastern part of İzmit Mainshock. Then normal values are recovered at the depth of 10 km. In the 3rd layer, namely 10 km depth in the southern part of Gemlik, also
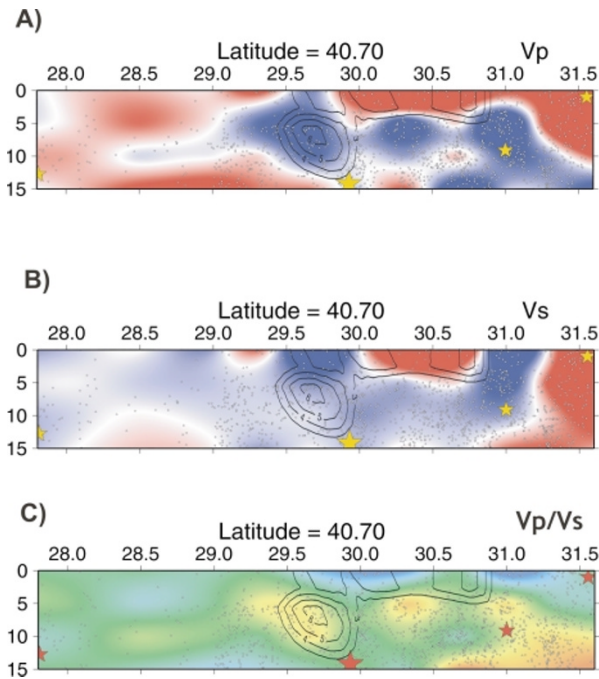
Fig. 10. Vertical cross section of velocity perturbation in the east-west direction along 40.70°N for (a) the *P* wave, (b) the *S* wave and (c) Vp/Vs. Scales for color shading are the same as given in Fig. 7. The relocated hypocenters (black dots) and the used seismic stations (dark yellow reverse triangles) are also shown. Contours show the distribution of coseismic slip obtained by Yagi and Kikuchi (2000). The counter interval is 1 m. Yellow stars in (a) and (b), and red stars in (c) show the Izmit mainshock and moderate aftershocks.

exits an area of lower values. In 15 km depth slice, we can see lower anomalies at Çinarcik Basin, ArmutlıPeninsula, Izmit Bay and Iznik Lake regions. On the other hand, we find a very high value area in the west of the Duzce region at 5 km depth and it becomes wider at 10 km depth. At this depth we also see another high value area located around the south of Akyazi. At the 15 km depth layer, these high value areas are reduced, and in the Iznik Lake, and Çinarcik, low values again prevail. The low Vp/Vs anomalies in the northern and eastern portions of the study region are in good agreement with sedimentary layers and alluviums.

We now examine the cross sections of velocity perturbation in the east-west direction along the NAFZ and in the north-south directions crossing the mainshock regions of the recent large earthquakes which occurred in 1999. In Fig. 10, we show the E-W cross sectional view of velocity perturbation along 40.7°N for (a) the *P* wave, (b) the *S* wave and (c) Vp/Vs. The slip distribution for the Izmit earthquake obtained by Yagi and Kikuchi (2000) is also shown. As we can see in Fig. 10(a), the hypocenter is located at the high-velocity side of the transition between the low and high *P*-wave velocity perturbations. As for the *S*-wave perturbation, we find a different pattern for the Izmit earthquake. The hypocenter of the Izmit earthquake is located in the higher velocity zone, as clearly seen in Fig. 10(b). As for Vp/Vs values, one of the recent mainshocks and most of the moderate aftershocks are located between the high and low velocity zones with moderate Vp/Vs as 1.73. The results shown here will be discussed
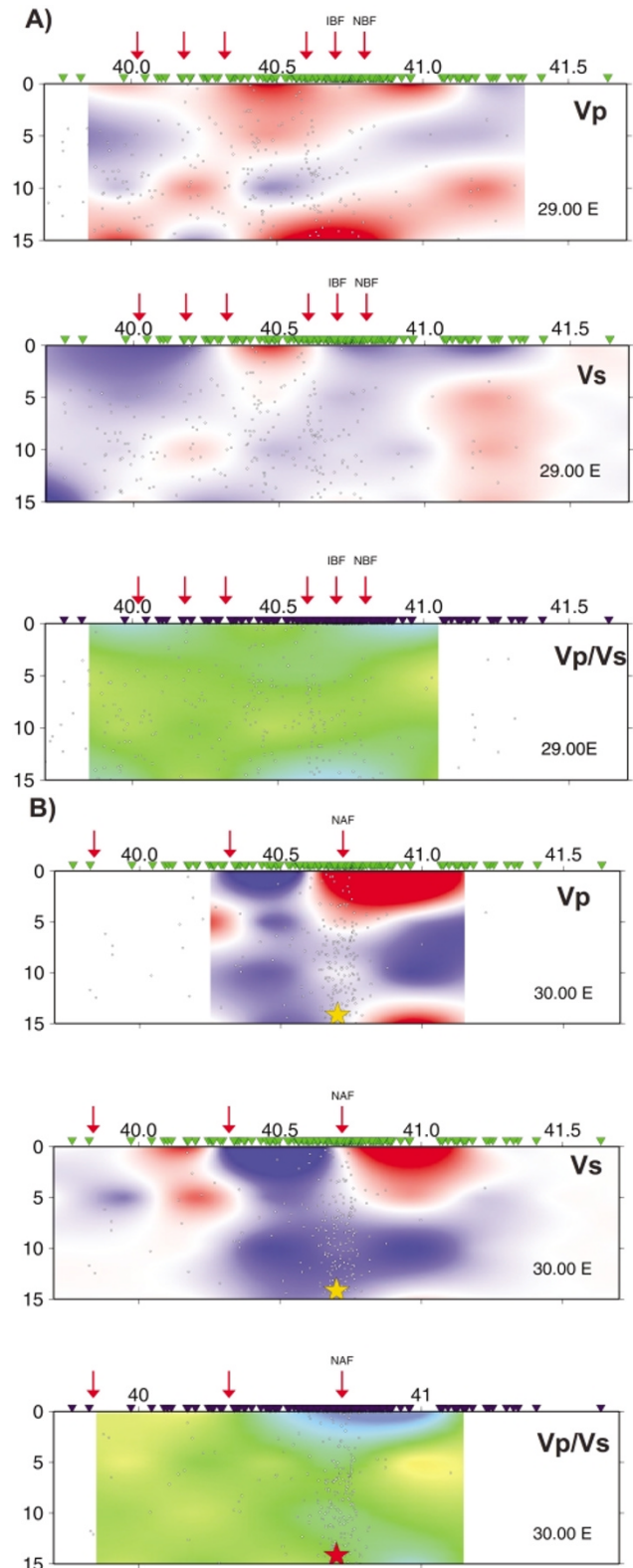

Fig. 11. Vertical cross sections of velocity perturbation in the north-south direction along (a) 29.0°E, (b) 30.0°E and (c) 31.33°E for the *P* and *S* waves and the Vp/Vs ratio, respectively. Symbols and color shading for velocities are the same as in Figs. 7 and 9. Red arrows show the active faults.

in more detail in the following section.

In this cross section, it is also shown that the sedimentary layers in the eastern part of the Marmara Sea region seem
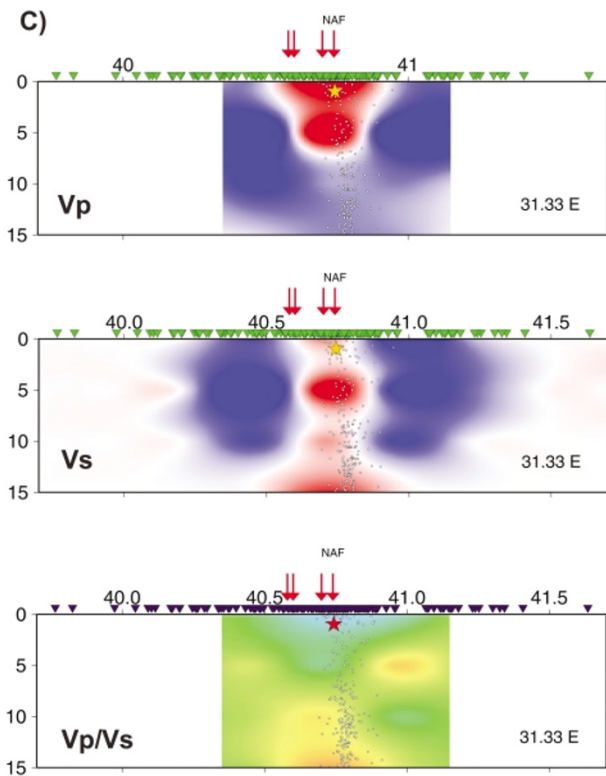
Fig. 11. (continued).

to extend down to 15 km depth. We can also clearly see around 5 km thick, low *P*-velocity anomaly extending from 29.8°E to the eastern end of the study region. This low velocity anomaly increased up to 12 km in the most eastern part of the study region. It should be noted that this area is covered with the Holocene alluvium (Aydin and Kalafat, 2002) and our results are quite consistent with the geology of this region.

The initial hypocenters turned out to be similar to the relocated hypocenters, which are shown in Fig. 2. Also we can see no clear relation between the seismicity and the velocity pattern, contrary to the relation found in California (Zhao and Kanamori, 1993). A similar less marked variation of hypocenters has been reported by Eberhart-Phillips (1986, 1989, 1990) and Michael (1988). We pointed out that the station density is generally poor in the western part of the study region, but we can also see no clear relation even in the area where the density of seismic station is very high and the number of aftershocks is very large. So we presume that such a result would be due to the geological structure, which is more complex than the San Andreas Fault. In any case, the results of seismic explosion experiments should be useful to check the reliability of the initial velocity model and the relocation procedure, although they have not been available yet for the whole area.

We also tried to examine a possible relation of the occurrences of large and moderate earthquakes with the velocity patterns. Fig. 10(a) indicates that most of the events listed in Table 2 tend to be located in high *Vp* zones or in transition zones between low and high *P*-wave velocity anomalies. These results are in good agreement with those obtained by

Hauksson and Hasse (1997). The events larger than 15 km hypocenter depth are not discussed in the text. More detailed discussion will be given later.

We also obtained cross sections in the north-south direction, especially for the Izmit and Duzce earthquake areas. In Figs. 11(a), (b) and (c), we show the cross sections along 29.0°E, 30.0°E and 31.33°E, respectively. One distinct feature of seismicity is that the earthquake distribution is sparse along the cross section of 30.0°E, as seen in Fig. 11(b), but it is more confined along 31.33°E with the dip angle of about 85°, as seen in Fig. 11(c). When we carefully inspect the earthquake distribution along the cross section of 29.0°E in the N-S direction, as shown in Fig. 11(a), the diffused seismicity pattern does not supports the idea of Okay *et al.* (2000) that the Çinarcik basin and the Inner Boundary Fault merge with the Northern Boundary Fault at the depth of about 10 km with a single fault trace below that depth.

5. Interpretations with Particular Reference to Other Observations

For interpretations of the results of tomography, comparisons with other geological and geophysical observations should be important. Especially, in the tectonically complex Marmara Sea region, the other pieces of information are necessary to examine the reliability of the tomography results. In this section, therefore, we will compare our results with an earlier tomographic work, some magnetotelluric (MT) profiles, gravity anomalies, and magnetic anomalies.

We first compare our results with the tomography work of Nakamura *et al.* (2002). We first point out that the rms values are almost halves of those of Nakamura *et al.* (2002) for the *P* wave, in spite of larger estimated reading errors for our data set. We found that our final velocity patterns are similar to their results even though they used a different data set, a different velocity model and a different relocation procedure. For example, the hypocenter of the Izmit mainshock is located in a relatively high velocity area between two low velocity areas. Also there is another high velocity zone at depths of 5 and 10 km in the east of 29.4°E. The main difference is that there is no low velocity zone above the Izmit mainshock in our results compared with the result of Nakamura *et al.* (2002), in which a low velocity zone in the first layer is absent. In our result, another relatively high velocity anomaly exists between the low velocity zone in the top layer and the low velocity zone just above the hypocenter of the Izmit earthquake. This difference stems probably from denser grid spacing, both horizontally and vertically, more seismic stations and more earthquakes in our work. The highest slip is seen in the high velocity anomaly and the rupture stopped near the low velocity anomaly in the west, as pointed out by Nakamura *et al.* (2002).

The seismic velocity is related to the density and there is a general correlation between the gravity and the velocity; high velocities are associated with high gravity values and low velocities with low gravity values. Thurber (1993) showed a rough correlation between velocities and gravity anomalies at the depth range from the near surface to 7 km depth in California. In fact, gravity values are estimated from velocity values (Eberhart-Phillips, 1993). Therefore,
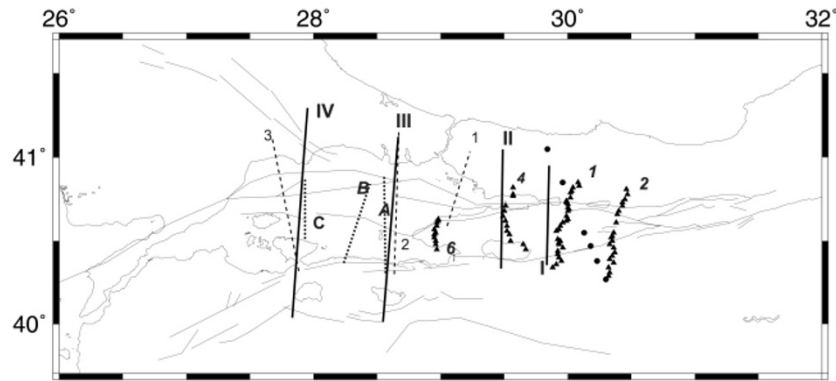
Fig. 12.   Locations of seismic, Bouguer gravity, geomagnetic and magnetotelluric (MT) observations made by some researchers in the Marmara Sea region. The same profiles are considered for the velocity perturbations through interpolation. The seismic and magnetic observations conducted along profiles I-IV (thick solid lines) are given in Ateş *et al.* (2003). The seismic, gravity and magnetic observations made along profiles A-C (thick dashed lines) are given in Adatepe *et al.* (2002). The gravity and magnetic observations made along profiles 1–3 (thin dashed lines) are given in Özer *et al.* (2001). The profiles 1, 2, 4, and 6 (solid triangles) show the MT observation points for Tank (2002, personal communication) and Tank *et al.* (2003) and solid circles for Gürer (1996). Symbols and color shading for velocities are the same as in Figs. 7 and 9.

Table 2.   List of the Izmit and the Duzce mainshocks and the selected moderate earthquakes which occurred in the Marmara region. The hypocenter parameters were obtained from the 3-D inversion result.

| Date | Origin Time | Location | | Depth | Magnitude |
Year Mo Dd	Hh:mm	Lat. (N)	Lon. (E)	km	Mw
1999 08 17	00.30	40.7005	29.9310	14.18	7.4
1999 08 17	21:14	40.6951	30.2673	21.14	4.5
1999 11 11	14:41	40.7699	30.2802	18.19	4.8
1999 11 11	16:57	40.8151	31.1641	17.93	7.2
1999 11 16	17:51	40.7430	31.5557	0.98	4.6
1999 11 19	19:59	40.8129	30.9993	9.14	4.5
2002 03 23	02:36	40.8230	27.8097	12.76	4.7

tomography results should be compared with the gravity data to evaluate the results more precisely in terms of the density.

Here we compare our results with several gravity profiles available for the Marmara Sea region (Adatepe *et al.*, 2002; Özer *et al.*, 2001; and Ateş *et al.*, 2003). The locations of the profiles are shown in Fig. 12. We estimated the velocity perturbation along the gravity profiles by interpolating our velocity perturbation data at each grid point, as shown in Figs. 13, 14, and 15 for Adatepe *et al.* (2002), Özer *et al.* (2001) and Ateş *et al.* (2003), respectively. Adatepe *et al.* (2002) found low gravity values for the Miocene-Pliocene sedimentary sequences and higher values for the regions uplifted by deformation. The velocity perturbations along these profiles are rather well correlated with the sedimentary layers and uplifted regions mainly located in the north of the profiles; as seen in the cross sections, the sedimentary deposits are correspond to low velocity anomalies and the uplifted regions to high velocity anomalies.

When we compare our velocity patterns with the gravity and magnetic profiles in Ateş *et al.* (2003), we can see a similar correlation between the gravity and magnetic filed values and the velocity perturbations. For example, we can see a low velocity zone in the central part of the Marmara Sea. Ateş *et al.* (2003) pointed out that this region is a highly deformed zone, which is quite consistent with low velocity values. The tomographic results in the top layers are also in good agreement with their results in the Marmara

Sea (Profiles III and IV) and around Izmit (Profiles I and II). A similar rough correlation for the upper 10 km velocity perturbation with the gravity results of Özer *et al.* (2001) can be seen in Fig. 14.

The electrical resistivity usually derived from magnetotelluric observations is very sensitive to the fluid contents in the crust. We now compare our velocity perturbation values with the resistivity structure derived by Gürer (1996) and Tank *et al.* (2003). The locations of MT profiles are shown in Fig. 12 and the cross sectional views of the resistivity and the velocity perturbations are shown in Figs. 16, 17(a), (b), (c), and (d) for Gürer (1996), Tank (2002, personal communication) and Tank *et al.* (2003), respectively. We again obtained interpolated velocity values along the MT profiles. In general, high resistivity values represent compact rocks characterized by low porosity and the lack of fluid. On the other hand, lower resistivity values indicate high porosity with fluid, partial melting and/or high temperature. Low resistivity values at the top sedimentary layers correspond to the low velocity anomalies in the velocity cross section, especially in the plain areas, as pointed out earlier. In general, low resistivity values are consistent with low velocity anomalies in the deep crust. The difference in the vertical direction between MT and tomography inversion results is most probably due to different resolution in the methods.
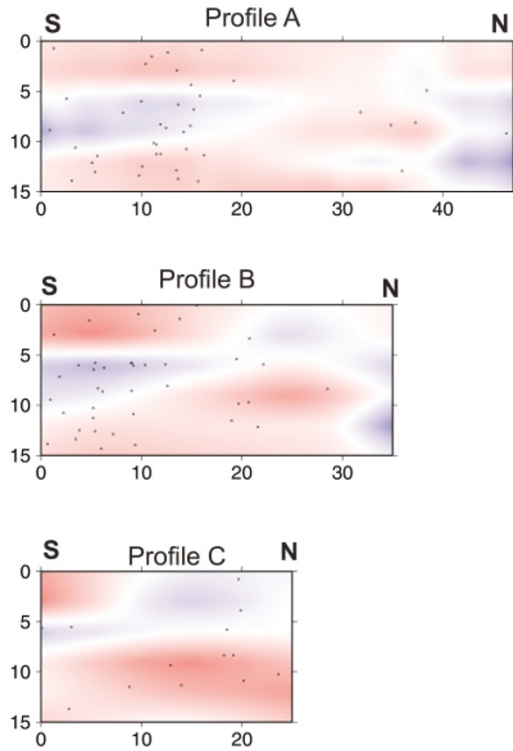
Fig. 13. Gravity data and structural models obtained along each profile, A-C, shown in Fig. 12 (Adatepe *et al.*, 2002). The corresponding *P*-wave velocity perturbations are shown below. Shading color scales are similar to those in Fig. 7.
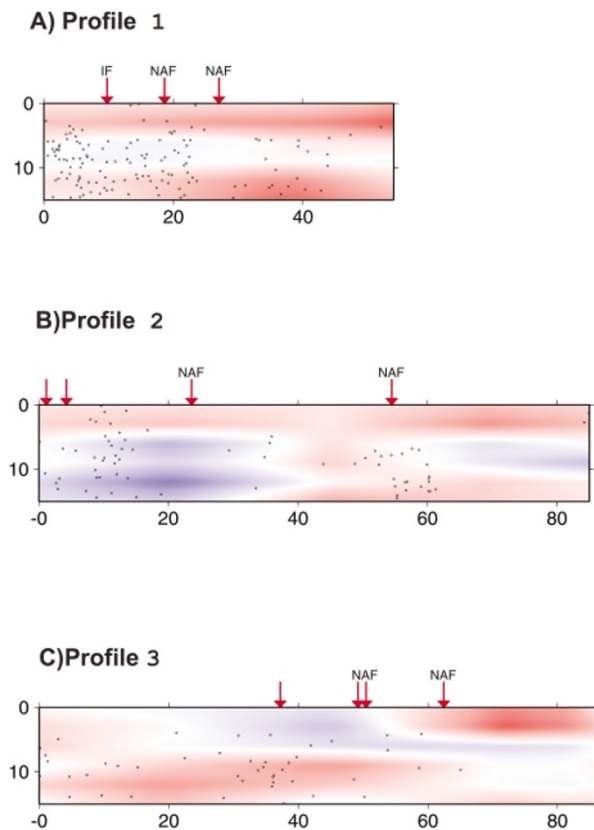

Fig. 14. Gravity data and structural models obtained along each profile, 1–3, shown in Fig. 12 (Özer *et al.*, 2001). The corresponding *P*- and *S*-wave velocity perturbations are shown below. Shading color scales are similar to those in Fig. 7.
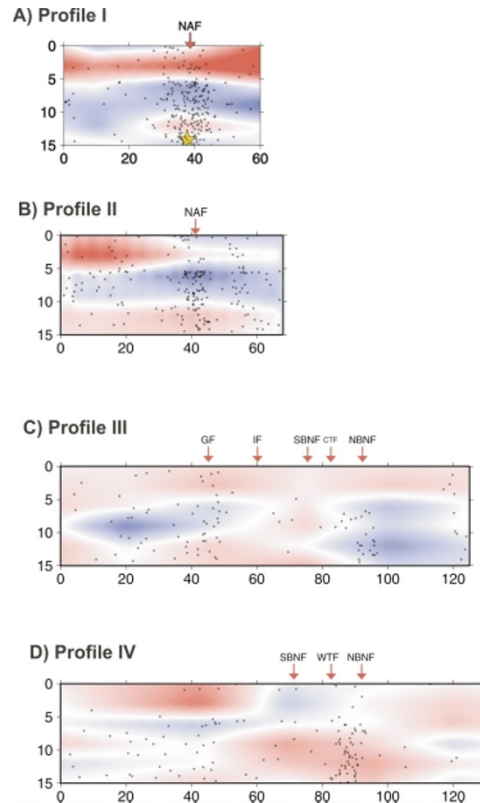

Fig. 15. Gravity and magnetic anomaly data along profiles I, II, III and IV shown in Fig. 12 (Ateş *et al.*, 2003). The corresponding *P*-wave velocity perturbations for each profile shown below. Dotted lines represent the marine Bouguer anomalies. NAF: North Anatolian Fault, GF: Gemlik Fault, NBNF: Northern Boundary North Anatolian Fault, IF: Imrali Fault, SBNF: South Boundary North Anatolian Fault, CTF: Çinarcik Transform Fault, WTF: Western Transform Fault. Shading color scales are similar to those shown in Fig. 7.
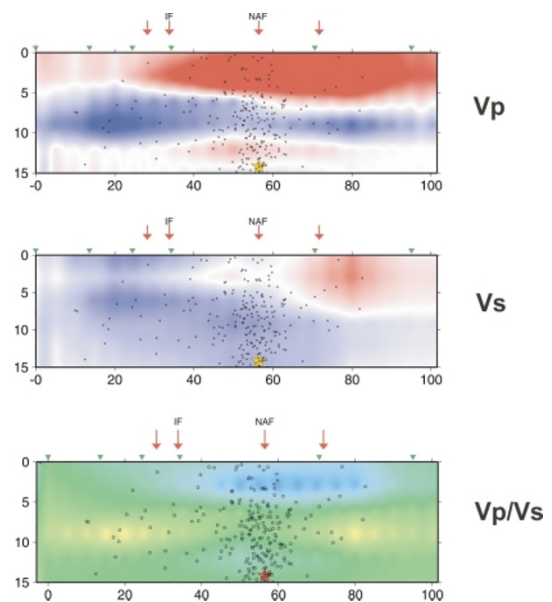

Fig. 16. The 2-D resistivity model obtained for the MT profile (Gürer, 1996). The velocity perturbations for the *P* wave, the *S* wave and the *Vp/Vs* values are shown along the MT profile. Color shading is given in Figs. 7, 8 and 9. Red arrows represent the active faults in the study area. The star symbol indicates the Izmit mainshock. IF: Iznik-Mekece Fault, NAF: North Anatolian Fault. Dark yellow inverted triangles represent the MT observation sites.

6. Discussion and Conclusions

The data for the present tomography study consist of earthquakes occurring in the Marmara Sea region and two recent strong earthquakes and their aftershocks, recorded by different networks and field campaigns of various research groups. We combined most of the available data for the Marmara region, including aftershocks of the Izmit and the Duzce earthquakes. We first relocated the hypocenters from all the available phases by using the 1-D velocity model, which has been widely used by KOERI for the Marmara region. We selected a 3-D grid and the events, depending upon several criteria for tomographic inversion. By applying a 3-D tomographic inversion technique called TOMOG3D, developed by Zhao *et al.* (1992) and widely used since then, to the travel time data for local earthquakes in the Marmara Sea region, we could determine velocity perturbation of this region and relocate 3,949 earthquakes selected for the period from 1985 to 2002. The average root mean square (RMS) values for the travel times decreased from 0.159 sec to 0.154 sec for the *P*-wave data and from 0.161 sec to 0.159 sec for the *S*-wave data. The obtained velocity perturbation values show several distinctive features, as will be discussed in the following paragraphs.

In addition to various knowledge about tectonics and geology of the Marmara Sea region, there are many researches on the shallow structure from seismic prospecting (Okay *et al.*, 2000; Alpar and Yaltirak, 2002; Adatepe *et al.*, 2002; Demirbağ *et al.*, 2003; Ateş *et al.*, 2003; Özer *et al.*, 2001) and some drilled wells for oil exploration. However, the deep structure in the Marmara Sea has not been well known. It is important to identify structural features such as high velocity anomalies along faults under the Sea of Marmara which may be a potential fault-rupture area causing major earthquakes. In this respect, we observed high and low velocity zones in the region and strong lateral variations at different depth slices as well as vertical variations of velocity perturbation in the E-W and the N-S directions. Furthermore, the relocated seismicity shows that the NAFZ in the Marmara Sea region appears as complicated as described in the geological, tectonical and seismic studies. For example, the low velocity zones at hypocentral depth beneath the middle Marmara Sea could be explained by high thick sedimentary units, by heterogeneity of material, by the presence of fluids, by high pore pressure, or by the combination of these. In fact, Nakamura *et al.* (2002) concluded that the low velocity anomalies found near the Izmit mainshock area correspond to high-porosity zones without interconnected fluids.

Meade *et al.* (2002) concluded that the northern branch of the NAFZ is more active as clearly shown by relative motion of about 24 mm/year which has been disclosed by GPS observations. This conclusion was also supported by Reilinger *et al.* (1997), McClusky *et al.* (2000) and Ayhan *et al.* (2002). Meade *et al.* (2002) pointed out that the strain accumulation in the Marmara Sea region is highly localized along the straight fault geometry with a shallow locking depth of 6–7 km. Ayhan *et al.* (2002) concluded that the largest shear-strain accumulation is seen along the northern branch of the NAFZ with a maximum shear-strain rate reaching 220 nanostrain/year in the Marmara Sea. The present seismicity distribution given in Fig. 3 is very consistent with these results. Most of the microearthquake activities are located along the northern branch. On the other hand, most of the seismicity along the western part of the NAFZ concentrates below this depth. Probably the creep may be confined to the upper portion of the NAFZ and the seismogenic zone of the fault extending from 7 to 15 km would be locked to store strain for future earthquakes.

Microearthquake activity, long-term seismicity, high slip-rate and seismic migration of large earthquakes at the NAFZ suggest that the Marmara Sea region is a potential site for the next large earthquake. Toksöz *et al.* (1979) pointed out that an almost 300 km long segment of the NAFZ in the Marmara Sea region has not ruptured and can be identified as a seismic gap capable of generating a large earthquake. Even after the two recent large earthquakes in the east of the Marmara region, The Marmara Sea has been supposed to be a notable seismic gap along the NAFZ.

Zhao *et al.* (2000) claimed through tomographic studies that large earthquakes do not occur anywhere, but only in anomalous areas that may be detected by high-resolution seismic imaging with tomography and the combination with geophysical, geochemical and geological results. Eberhart-Phillips and Michael (1993) also claimed that high-velocity bodies correspond to hard asperities. A similar conclusion was derived by Young and Maxwell (1992); high seismic velocities characterize highly stressed regions and have a potential of significant seismic energy release. Lees (1990) and Zhao and Kanamori (1993) also concluded that most of the earthquakes in California (mainshocks and aftershocks) occur in high-velocity areas. These areas are probably strong brittle portions along the fault zone, while low velocity areas are probably weak ductile portions which cannot effectively generate earthquakes. Similar results can be found in Nicholson and Lees (1992), Eberhart-Phillips and Michael (1993), Hauksson and Hasse (1997) and Ishida and Hasemi (1998); earthquakes mostly occur in high velocity zones, and seismicity is low in low velocity zones. Nakamura *et al.* (2002) also suggested that the high velocity zone at the Iznik-Mekece fault might be broken easily in the future.

Thus it has widely been believed that defining such asperities by high velocity regions may help to predict the location and size of a future event along major strike-slip faults in California. On the other hand, Zhao and Negishi (1998), Zhao *et al.* (2000) and Zhao *et al.* (2001) pointed out through seismic tomography that many historical and recent interplate earthquakes in Japan occurred in or around the areas of low seismic velocity. These regions are supposed to represent decoupled, weak areas of the crust and the generation of a large earthquake is closely related to the physical and chemical properties of the material in the crust such as magma and fluids. In the case of northwestern Turkey, one recent large earthquakes and some strong aftershocks occurred in the high velocity (Vp) areas or the transition zone between high velocity and low velocity zones (see Fig. 7) in the eastern part of the studied area. In this respect, high velocity zones in the western extension of the NAFZ should be more important. We found some high Vp bodies at the Iznik-Mekece fault and the northern branch of the NAFZ
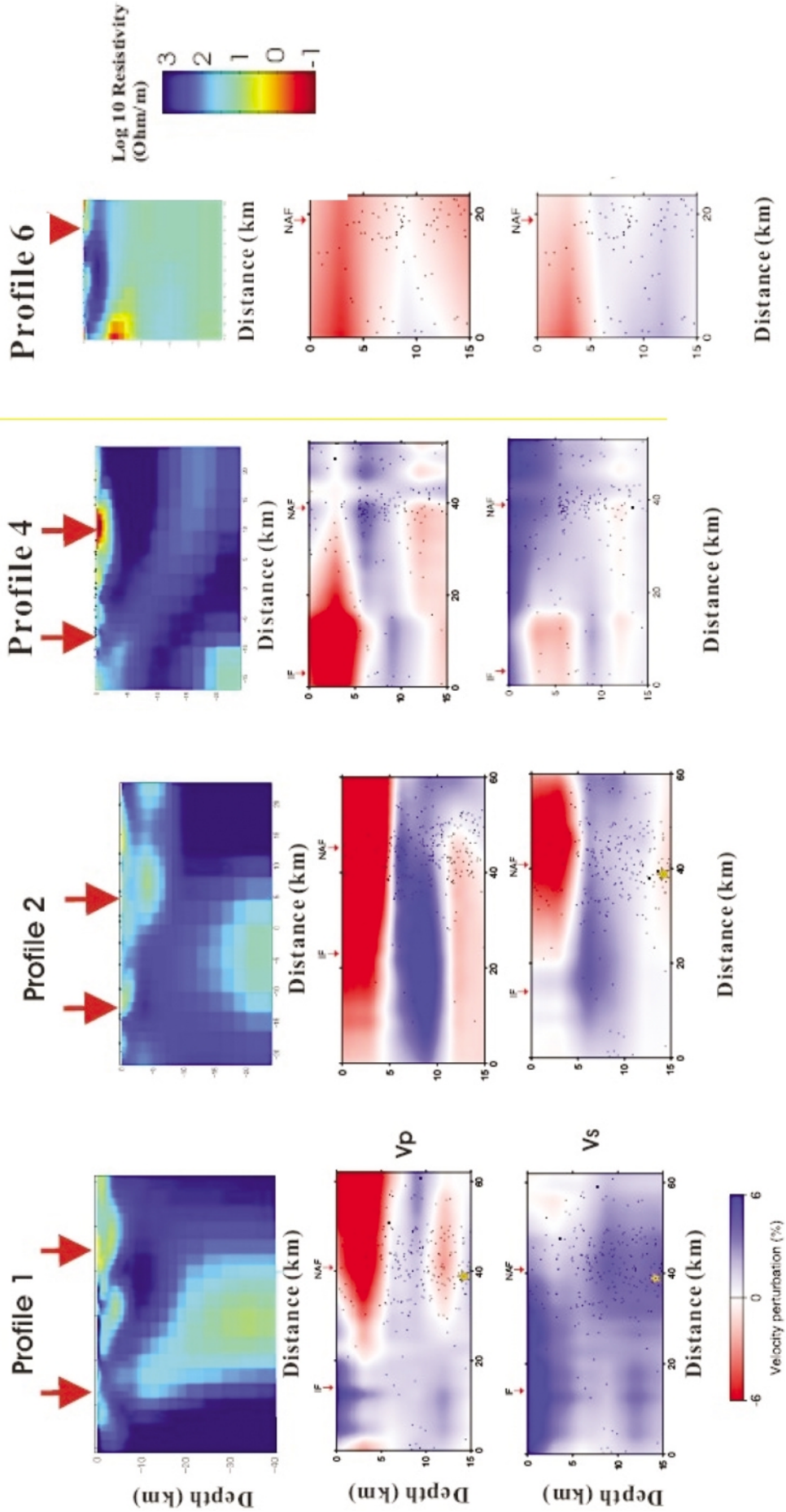
Fig. 17. Cross sections of the resistivity structure along (a) profile 1, (b) profile 2, (c) profile 4 and (d) profile 6 (Tank, 2002, personal communication; Tank *et al*., 2003). The corresponding *P*-wave and *S*-wave velocity perturbations for each profile are shown below. Red arrows indicate the active faults across the profile. Shading color scales are similar as those shown in Fig. 7.

passing trough the Marmara Sea. These regions could be possible sources of future large earthquakes and special attention is necessary to understand the relationship between the earthquake generation process and the inhomogeneity of the crust.

It should also be pointed out here that several low velocity anomalies were found. In particular, the sedimentary units or alluvium regions such as basins and plains in the Marmara region show lower Vp perturbations and low Vp/Vs values. On the other hand, the outcrop of volcanic rocks or granites and also volcanic and magmatic material situated in the deeper parts show higher Vp anomalies. Velocity perturbations from the initial model show that the low velocity zone in the central and western parts of the Marmara Sea continues to 15 km, deeper than expected. There is one relatively high velocity body at depth in 10 km at 28.0°E. The observed velocity perturbation structure is quite different for the Vs and the obtained Vp/Vs ratio also shows sharp lateral variations.

In the next, we compare the cross sections of the 3-D velocity structure with the hypocenters of the mainshock of the recent large earthquake, and its rupture areas given in Fig. 10. We then notice a strong lateral velocity variation across the fault at all the depths. For the Izmit earthquake, the high velocity zone at depths less than 5 km extending along the fault coincides with the area that is inferred to have ruptured during the mainshock. Larger slip occurred in the high velocity areas as clearly seen in Fig. 10(a). Delouis *et al.* (2002) concluded that a central asperity is located between 29.7°E and 30.4°E with slip reaching 6–8 m in the depth range of 5–10 km. We also considered the slip distribution for the Izmit earthquake reported by Yagi and Kikuchi (2000), and found a similar result; larger slip occurred in the higher velocity perturbation. We also found that the seismicity seems to diffuse into low and high velocity regions. There is no clear evidence showing that earthquakes clustering in high or low velocity zones. A similar conclusion was obtained by Eberhart-Phillips and Micheal (1993). It should be noted, however, that because of the poor station distribution in the western part of the Marmara Sea region, the structural resolution is not enough to have a better image of this portion.

The 3-D image presented here was also compared with the available gravity, MT and magnetic data. The observed Bouguer gravity values are supposed to roughly represent the density distribution of the upper crust. Thurber (1993) showed a rough correlation between velocities and gravity anomalies for the depth range from the near surface to 7 km depth in California, based on the computation of gravity values from the velocity as given in Eberhart-Phillips (1990). Hence, we attempted to compare our results with several gravity profiles obtained by Adatepe *et al.* (2002), Özer *et al.* (2001) and Ateş *et al.* (2003). Then we found that negative gravity anomalies are indicative of bifurcation of the NAF. The low-density sedimentary units could be the reason for the negative gravity anomalies. Also the local gravity anomalies show a particular correlation with the velocity perturbations. As for near-surface velocities, our model clearly shows the correlation with geology, the gravity and magnetic anomalies in the scale of horizontal block

size. High Vp and high gravity anomalies are associated with exposed metamorphic and magmatic rocks, and also alluvium or thick sedimentary units in the basins like Iznik, Karacabey or Çinarcik in the Marmara Sea are associated with low velocity, low gravity and low resistivity. There is a high magnetic anomaly appearing from the entrance of the Bosphorus and reaching the south of Tekirdağ. This high anomaly is supposed to have originated from Precambrien metamorhpites underlain by Paleozoic rocks. This region shows higher velocity perturbations in slices 2 to 4 which are in good agreement with the magnetic anomalies for the uppermost layer. For higher magnetic anomalies observed along the profiles, high velocity perturbations tend to be seen in almost the same portion of the profiles.

MT sounding is a very useful and powerful tool for crustal studies in earthquake source regions, since the resistivity is sensitive to lateral structural variations. Mafic rocks are usually characterized by high-velocity and high-resistivity blocks, whereas sediments or alluviums by low velocity and low resistivity. Unsworth *et al.* (2000), Mitsuhata *et al.* (2001) and Ogawa *et al.* (2001, 2002) all showed that seismic activity clusters near the rims of low resistivity zones. This result also holds for the Izmit and the Duzce earthquakes. Gürer (1996) pointed out that the Iznik metamorphic assemblage and the Geyve ophiolite are very resistive, and showed that the sedimentary layers are about 4 km thick in Izmit and 2 km thick in Geyve. Gürer (1996) also found very conductive zones in the top layer and conductive zones in deeper parts. Tank *et al.* (2003) also concluded that most of the aftershocks tended to occur in a resistive zone underlain by a moderately conductive zone. Nakamura *et al.* (2002) concluded that many aftershocks tended to occur at the edge of high resistivity anomaly, comparing velocity perturbation, relocated seismicity and the resistivity structure reported by Oshiman *et al.* (2002). These results indicate that material property is heterogeneous along the NAFZ.

Tank *et al.* (2002, personal communication), in addition to reevaluation of the data set obtained by Oshiman *et al.* (2002), made new observations along the same profile and along a new profile. They found a remarkable relation between seismic activity and the resistivity structure; aftershocks of the Izmit earthquake tended to occur in the resistive zone underlain by a moderately conductive zone. Such a relation between seismicity and the resistivity structure has also been reported in seismically active areas in Japan (Mitsuhata *et al.*, 2001; Ogawa *et al.*, 2001, 2002). The resistivity structure and the velocity perturbation are shown in Figs. 16, 17(a), (b), (c) and (d), indicating good correlation between each other. High Vp anomalies correspond to high resistive zones and low velocity anomalies to low resistive zones.

It should be noted, however, that for MT profile 2, a different feature was seen; the seismic activity is in fact regarded as an earthquake swarm and it is related to crustal fluid existing in the low resistivity area. Such crustal fluid is supposed to trigger the swarm activity. However, we obtained higher S-wave velocity perturbation and lower Vp/Vs ratio for this region. Hence one possible cause of this conductive zone is lithological complexity of the mate-

rial, high metamorphism or higher degree porous material in the crust. Alternatively, the inversion may have been influenced by strong anisotropy of seismic wave velocities.

We have also tried to evaluate Vp/Vs values by using P- and S-wave data in the present study. Vp/Vs ratio, which also corresponds to the Poisson ratio, provides the information on rock property, fluid content and partial melting. High Vp/Vs values are supposed to be associated with highly fractured and water-saturated rocks. Lowering of Vp/Vs corresponds to closing of microcracks under increasing confining pressure. In volcanic regions, low Vp, low Vs and high Vp/Vs often indicate partial melting. Vp/Vs is also very sensitive to the silica content of volcanic rocks. For example, Christensen (1996) showed that for rocks with SiO_2 content above 55% and to 75%, compressional wave velocities decrease and shear velocities increase with increasing percentage of SiO_2. According to this result, the seismic velocity at the Mesozoic/Cenozoic orogenic belts should be low, compared with the shield regions. On the other hand, high fluid pressure would reduce Vp and increase Vp/Vs.

Walck (1988) pointed out that shallow microearthquakes tend to occur in low Vp/Vs areas, whereas Nakajima *et al.* (2001) found that swarms occur in areas where Vp and Vs are slightly low and Vp/Vs is moderately low. Unfortunately, we could not find such a clear tendency between the seismicity and the Vp/Vs values. One possible reason for that is poor resolution of Vs, compared with Vp, because of smaller numbers of S-phase reading as well as different sets of stations for the S-wave data. Especially in the western and northwestern portions of the studied area, few seismic stations have been operated for a long time and even some of the key stations have provided S reading with rather poor accuracy. Therefore, we should be careful in interpreting Vp/Vs structures. Smaller Vp/Vs values could also be ascribed to artifacts caused by secondary early arrivals such as S to P converted phases, as discussed in Hauksson and Hasse (1997).

Since the Marmara Sea region is extremely important in that the potential of large earthquake occurrence is very high, more data are necessary, such as deep seismic refraction and reflection, sea bottom MT, dense microgravity survey and deep well data. A denser seismic network will allow us to have more detailed images of the faults zones in the study area. Better understanding of P- and S-wave velocity variations and Vp/Vs ratios is possible simply with addition of some new 3-component seismic stations to the present networks in the western part of the Marmara Sea region. In particular, ocean bottom seismometry (OBS) is vital to ensure denser grid spacing and accuracy of arrival times of S wave, without which high resolution of the crustal velocity structure in this region will not be attained.

References

Adatepe, F., S. Demirel, and B. Alpar, Tectonic setting of the southern Marmara Sea region based on seismic reflection data and gravity modelling, *Mar. Geol.*, **190**, 383–395, 2002.

Aki, K. and W. H. K. Lee, Determination of three-dimensional velocity anomalies under a seismic array using first P arrival times from local earthquakes, A homogeneous initial model, *J. Geophys. Res.*, **81**, 4381–4399, 1976.

Alpar, B. and C. Yaltirak, Characteristic features of the North Anatolian Fault in the eastern Marmara region and its tectonic evolution, *Mar. Geol.*, **190**, 329–350, 2002.

Ambraseys, N. N. and C. F. Finkel, Long-term seismicity of Istanbul and of the Marmara region, Engin. Seis. Earthq. Engin. Report, 91/8, Imperial Collage, 1991.

Ambraseys, N. N. and C. F. Finkel, *The Seismicity of Turkey and Adjacent Areas*, Eren Yayincilik, Istanbul, Turkey, 1995.

Ateş, A., T. Kayiran, and I. Şençer, Structural interpretation of the Marmara region, NW Turkey, from aeromagnetic, seismic and gravity data, *Tectonophysics*, **367**, 41–99, 2003.

Aydin, A. and D. Kalafat, Surface ruptures of the August and 12 November 1999 Izmit and Duzce earthquakes in northwestern Anatolia, Turkey: their tectonic and kinematic significance and associated damage, *Bull. Seism. Soc. Am.*, **92**, 95–106, 2002.

Ayhan, M. E., C. Demir, O. Lenk, A. Kiliçoğlu, Y. Altiner, A. A. Barka, S. Ergintav, and H. Özener, Interseismic strain accumulation in the Marmara Sea region, *Bull. Seism. Soc. Am.*, **92**, 216–229, 2002.

Barka, A., The North Anatolian Fault Zone, *Ann. Tectonicae*, **6**, 164–195, 1992.

Barka, A., The 17 August 1999 Izmit earthqauke, *Science*, **285**, 1858–1859, 1999.

Barka, A. A. and K. Kadinsky-Cade, Strike-slip fault geometry in Turkey and its influence on earthquake activity, *Tectonics*, **7**, 663–684, 1988.

Barka, A. A. and R. Reilinger, Active tectonics of the eastern Mediterranean region deduced from GPS, neotectonic, and seismicity data, *Annali Geofisica*, **40**, 587–610, 1997.

Bariş, Ş., S. B. Üçer, A. Ito, N. Kafadar, H. Alcik, A. Pinar, C. Gürbüz, Y. Honkura, and A. M. Işikara, Local microearthquake network in the western part of the North Anatolian Fault Zone, Japan Earth and Planetary Sciences Meeting, March, 26–29 1996, Osaka, Japan, 1996a.

Bariş, Ş., S. B. Üçer, A. Ito, C. Gürbüz, Y. Honkura, and A. M. Işikara, *IZINET: a digital seismic network along the North Anatolian fault in Turkey, Earthquake research in Turkiye State of the Art, Ankara, Turkey*, GFZ Publication 63, 1996b.

Bariş, Ş., A. Ito, S. B. Üçer, T. Komut, N. Kafadar, A. Ito, R. Pektaş, Y. Honkura, and A. M. Işikara, Microearthquake activity in the western extensions of the North Anatolian Fault Zone in the eastern Marmara region, Turkey (1993–1998), *Bull. Seism. Soc. Am.*, **92**, 394–405, 2002.

Bouchon, M., N. Toksöz, H. Karabulut, M. Bouin, M. Dietrich, M. Aktar, and M. Edie, Seismic imaging of the 1999 Izmit (Turkey) rupture inferred from the near-field recordings, *Geophys. Res. Lett.*, **27**, 3013–3016, 2000.

Canitez, N. and S. B. Üçer, Computer determinations for the fault plane solutions in and near Anatolia, *Tectonophysics*, **4**, 235–244, 1967.

Christensen, N. I., Poissons's ratio and crustal seismology, *J. Geophys. Res.*, **101**, 3139–3156, 1996.

Delouis, B., D. Giardini, P. Lundgren, and J. Salichon, Joint inversion of

InSAR, GPS, teleseismic, and strong-motion data for the spatial and temporal distribution of earthquake slip: application to the 1999 Izmit mainshock, *Bull. Seism. Soc. Am.*, **92**, 278–299, 2002.

Demirbağ, E., C. Rangin, X. Le Pichon, and A. M. C. Şengör, Investigation of the tectonics of the Main Marmara Fault by means of deep-towed seismic data, *Tectonophysics*, **361**, 1–19, 2003.

Dewey, J. H. and A. M. C. Şengör, Aegean and surrounding regions: complex multiplate and continuum tectonics in a convergent zone, *Geol. Soc. Am. Bull.*, Part I, **90**, 84–92, 1979.

Eberhart-Phillips, D., Three-dimensional velocity structure in northern California Coast Ranges from inversion of local earthquake arrival times, *Bull. Seismol. Soc. Am.*, **76**, 1025–1052, 1986.

Eberhart-Phillips, D., Active faulting and deformation of the Coalinga anticline as interpreted from three-dimensional velocity structure and seismicity, *J. Geophys. Res.*, **94**, 15565–15586, 1989.

Eberhart-Phillips, D., Three-dimensional P and S velocity structure in the Coalinga region, California, *J. Geophys. Res.*, **95**(B10), 15343–15363, 1990.

Eberhart-Phillips, D. and A. J. Michael, Three-dimensional velocity structure, seismicity, and fault structure in the Parkfield region, Central California, *J. Geophys. Res.*, **98**, 15767–15758, 1993.

Ergin, M., M. Aktar, F. Bicmen, A. Yoruk, N. Yalcin, and S. Kuleli, Microearthquake study of Izmit Bay, presented at the Active Tectonics Meeting Proc., Vol. 1, Istanbul Technical University, Istanbul, Turkey, 2000.

Eyidoğan, H., A. Çisternaş, C. Gürbüz, M. Aktar, H. Haesler, N. Turkelli, F. Bicmen, S. B. Üçer, S. Kuleli, A. Barka, A. M. Işikara, O. Polat, B. Kaypak, M. Ergin, E. Arpat, A. Yoruk, Ş. Bariş, D. Kalafat, H. Alcik, A. Güngör, S. Ince, E. Zor, T. Bekler, R. Gok, G. Gorgulu, and M. Kara, *Marmara Denizi ve Cevresindeki Mikro-Deprem Arastirmasinin Sonuclari*, IU DBE Vefa Toplantisi, Istanbul, 1998 (in Turkish).

Finkel, C. F., Earthquakes of the Marmara Sea basin: reflections on the need for co-operation between historian and scientist, 101–111, in *Integration of Earth Science Research on the Turkish and Greek 1999 earthquakes*, edited by N. Gorur, G. A. Papadopoulos and N. Okay, Kluwer Academic Pub., 207 pp., NATO Science series IV. Earth and Environmental Sciences Vol. 9, 2002.

Genç, M. and M. Mazak, *Istanbul Depremleri*, IGDAS Publication, Istanbul, Turkey, 2001.

Gürbüz, C., M. Aktar, H. Eyidoğan, A. Çisternaş, H. Haessler, A. Barka, M. Ergin, N. Turkelli, O. Polat, S. B. Üçer, S. Kuleli, Ş. Bariş, B. Kaypak, T. Bekler, E. Zor, F. Bicmen, and A. Yoruk, Seismotectonics of the Marmara region (Turkey): results from a microseismic experiment, *Tectonophysics*, **316**, 1–17, 2000.

Gürbüz, C., H. S. Kuleli, T. Bekler, E. Zor, H. Karabulut, and M. Zobu, Crustal structure studies in western Turkey based on earthquake and explosion seismic data, XXVI. General Assembly of The European Seismological Commission (ESC), International Association of Seismology and Physics of The Earth's Interior (IASPEI), International Union of Geodesy and Geophysics (IUGG), 1998.

Gürer, A., Deep conductivity structure of the North Anatolian Fault Zone and the Istanbul and Sakarya Zone along the Geyve-Akcakoca profile, northwest Anatolia, *Int. Geology Rev.*, **38**, 727–736, 1996.

Hauksson, E. and J. S. Hasse, Three-dimensional Vp and Vp/Vs velocity models of the Los Angeles basin and central Transverse Ranges, California, *J. Geophys. Res.*, **102**, 5423–5453, 1997.

Honkura, Y. and A. M. Işikara, Multidisciplinary research on fault activity in the western part of the North Anatolian Fault Zone, *Tectonophysics*, **193**, 347–357, 1991.

Honkura, Y., A. M. Işikara, D. Kolçak, N. Orbay, S. Sipahioğlu, N. Ohshiman, and H. Tanaka, Magnetic anomalies and low ground resistivity as possible indicators of active fault location: preliminary results of electric and magnetic observations from the western part of the North Anatolian Fault Zone, *J. Geomag. Geoelectr.*, **37**, 169–187, 1985.

Honkura, Y., A. M. Işikara, N. Oshiman, A. Ito, B. Üçer, Ş. Bariş, M. K. Tunçer, M. Matsushima, R. Pektaş, C. Çelik, S. B. Tank, F. Takahashi, R. Yoshimura, Y. Ikeda, and T. Komut, Preliminary results of multidisciplinary observations before, during and after the Kocaeli (Izmit) earthquake in the western part of the North Anatolian Fault Zone, *Earth Planets Space*, **52**, 293–298, 2000.

Horasan, G., L. Gülen, A. Pinar, D. Kalafat, N. Özel, H. S. Kuleli, and A. M. Işikara, Lithosperic structure of the Marmara and Aegean regions, western Turkey, *Bull. Seism. Soc. Am.*, **92**, 322–329, 2002.

Humphreys, E. and R. W. Clayton, Adaptation of back projection tomography to seismic travel time problems, *J. Geophys. Res.*, **93**, 1073–1085, 1988.

Iio, Y., S. Horiuchi, Ş. Bariş, C. Çelik, J. Kyomen, B. Üçer, Y. Honkura, and A. M. Işikara, Aftershock distribution in the eastern part of the aftershock region of the 1999 Izmit, Turkey, earthquake, *Bull. Seism. Soc. Am.*, **92**, 418–427, 2002.

Ikeda, Y. and T. Komut, Surface ruptures associated with the Kocaeli, northwestern Turkey, earthquake of August 17, 1999 (abstracts), *J. Seism. Soc. Jpn.*, 1999 Fall meeting, A64, 1999 (in Japanese).

Ikeda, Y., Y. Suzuki, and E. Herece, Late Holocene activity of the North Anatolian Fault Zone in the Orhangazi Plain, in *North Western Turkey, Multidisciplinary Research on Fault Activity in the Western Part of the North Anatolian Fault Zone (2)*, edited by Y. Honkura and A. M. Işikara, pp. 16–30, Tokyo Inst. Tech., 1989.

Inoue, H., Y. Fukao, K. Tanabe *et al.*, Whole mantle P-wave travel time tomography, *Phys. Earth Planet. Inter.*, **59**, 294–328, 1990.

Ishida, M. and A. K. Hasemi, Three-dimensional fine velocity structure and hypocentral distribution of earthquakes beneath the Kanto-Tokai district, Japan, *J. Geophys. Res.*, **93**, 2076–2094, 1998.

Işikara, A. M., Y. Honkura, N. Watanabe, N. Orbay, D. Kolçak, N. Ohshiman, O. Gündoğdu, and H. Tanaka, Magnetic anomalies in the western part of the North Anatolian Fault Zone and their implications for active fault structure, *J. Geomag. Geoelectr.*, **37**, 541–560, 1985.

Ito, A., C. Gürbüz, S. B. Üçer, Ş. Bariş, H. A. Alçik, Y. Honkura, and A. M. Işikara, Seismic observation in the western part of the North Anatolian Fault Zone, in *Multidisciplinary Research on Fault Activity in the Western Part of the North Anatolian Fault Zone*, edited by Y. Honkura and A. M. Işikara, **5**, pp. 23–32, Boğaziçi University Publ., 1994.

Ito, A., S. B. Üçer, Ş. Bariş, Y. Honkura, A. Nakamura, T. Kono, R. Pektaş, T. Komut, A. Hasegawa, and A. M. Işikara, Preliminary Report on the aftershocks of August 17, 1999 Izmit Earthquake, Turkey, revealed from micro-earthquake observations, in *The 1999 Izmit and Duzce Earthquakes: Preliminary Results*, edited by A. Barka, O. Kozaci, S. Akyuz, and E. Altunel, Istanbul Teknik Univ. Yayini, Istanbul, 2000.

Ito, A., S. B. Üçer, Ş. Bariş, A. Nakamura, Y. Honkura, T. Kono, S. Hori, A. Hasegawa, R. Pektaş, T. Komut, and A. M. Işikara, Aftershock activity of 1999 Izmit earthquake, Turkey, revealed from microearthquake observations, *Bull. Seism. Soc. Am.*, **92**, 418–427, 2002.

Kissling, E., W. L. Ellsworth, D. Eberhart-Phillips, and U. Kradolfer, Initial reference models in local earthquake tomography, *J. Geophys. Res.*, **99**, 19635–19646, 1994.

Kuleli, H. S., C. Gürbüz, and M. N. Toksöz, Seismic velocity distribution in the Aegean region, IESCA-1995 Proceedings, 1995.

Lee, W. H. K. and J. C. Lahr, HYP071 (Revised): a computer program for determining hypocenter, magnitude, and first motion pattern of local earthquakes, U. S. Geological Survey Open File Report 75-311, 113 pp., 1975.

Lee, W. H. K. and C. M. Valdes, HYP071PC: a personal computer version of the HYPO71 earthquake location program, U. S. Geological Survey Open File Report 85-749, 43 pp, 1985.

Lees, J. M., Tomographic P-wave velocity images of the Loma Prieta earthquake asperity, *Geophys. Res. Lett.*, **17**, 1433–1436, 1990.

McClusky, S., S. Balassanian, A. Barka, C. Demir, S. Ergintav, I. Georgiev, O. Gürkan, M. Hamburger, K. Hurst, H. Kahle, K. Kastens, G. Kekelidze, R. King, V. Kotzev, O. Lenk, S. Mahmoud, A. Mishin, M. Nadariya, A. Ouzounis, D. Paradissis, Y. Peter, M. Prilepin, R. Reilinger, I. Sanli, H. Seeger, A. Tealeb, M. N. Toksöz, and G. Veis, Global positioning system constraints on plate kinematics and dynamics in the eastern Mediterranean and Caucasus, *J. Geophys. Res.*, **105**, 5695–5719, 2000.

McKenzie, D. P., Active tectonics of Mediterranean region, *Geophys. J. R. Ast. Soc.*, **30**, 109–185, 1972.

Meade, B. J., B. H. Hager, S. C. McClusky, R. E. Reilinger, S. Ergintav, O. Lenk, A. Barka, and H. Ozener, *Bull. Seism. Soc. Am.*, **92**, 208–215, 2002.

Michael, A. J., Effects of three-dimensional velocity structure on the seismicity of the 1984 Morgan Hill, California, aftershock sequence, *Bull. Seismol. Soc. Am.*, **78**, 1199–1221, 1988.

Mitsuhata, Y., Y. Ogawa, M. Mishina, T. Kono, Y. Yokokura, and T. Ushida, Eectromagnetic heterogeneity of the seismogenic region of 1962 M6.5 Northern Miyagi Earthquake, northeastern Japan, *Geophys. Res. Lett.*, **28**, 4371–4374, 2001.

Nakajima, J., T. Matsuzawa, D. Zhao, and A. Hasegawa, Three-dimensional structure of Vp, Vs, and Vp/Vs beneath northeastern Japan: implications for arc magmatism and fluids, *J. Geophys. Res.*, **106**, 21843–21857, 2001.

Nakamura, A., A. Hasegawa, A. Ito, S. B. Üçer, Ş. Bariş, Y. Honkura, T.

Kono, S. Hori, R. Pektaş, T. Komut, C. Çelik, and A. M. Işikara, P-wave velocity structure of the crust and its relationship to the occurrence of the 1999 Izmit, Turkey earthquake and aftershocks, *Bull. Seism. Soc. Am.*, **92**, 330–338, 2002.

Nicholson, C. and J. M. Lees, Travel-time tomography in the northern Coachelle Valley using aftershocks of the 1986 ML 5.9 North Palm Springs earthquake, *Geophys. Res. Lett.*, **19**, 1–4, 1992.

Ogawa, Y., M. Mishina, T. Goto, H. Satoh, N. Oshiman, T. Kasaya, Y. Takahashi, N. Nishitani, S. Sakanaka, M. Uyeshima, Y. Takahashi, Y. Honkura, and M. Matsushima, Magnetotelluric imaging of fluids, in intraplate earthquake zones, NE Japan back arc, *Geophys. Res. Lett.*, **28**, 3741–3744, 2001.

Ogawa, Y., S. Takakura, and Y. Honkura, Resistivity structure across Itoigawa-Shizuoka tectonic line and its implications for concentrated deformation, *Earth Planets Space*, **54**, 1115–1120, 2002.

Okay, A., E. Demirbağ, H. Kurt, N. Okay, and I. Kuscu, An active deep-marine strike-slip basin along the North Anatolian fault in Turkey, *Tectonics*, **18**, 129–147, 1999.

Okay, A. I., A. Kaslilar-Ozcan, C. Imren, A. Boztepe-Güney, E. Demirbağ, and I. Kuscu, Active faults and evolving strike-slip basins in the Marmara Sea, northwest Turkey: a multichannel seismic reflection study, *Tectonophysics*, **321**, 189–218, 2000.

Oral, B., R. Reilinger, M. N. Toksöz, R. W. King, A. Barka, I. Kinik, and O. Lenk, Global positioning system offers evidence of plate motion in Eastern Mediterranean, *EOS Trans. AGU*, **76**(2), 9–11, 1995.

Oshiman, N., Y. Honkura, M. Matsushima, Ş. Bariş, C. Celik, M. K. Tunçer, and A. M. Işikara, Deep resistivity structure around the fault associated with the 1999 Kocaeli earthquake, Turkey, in *Seismotectonics in Convergent Plate Boundary*, edited by Y. Fujiwara and Y. Yoshida, pp. 293–303, Terra Scientific Publishing Company, Tokyo, 2002.

Özer, N., M. Hisarli, D. Kolçak, Z. Duzgit, B. Tok, and M. Tankut, Seismicity of the Marmara Region and it's indications concerning the other geophysical and geological findings, *EOS Trans. AGU*, **82**(47), F936, 2001.

Paige, C. C. and M. A. Saunders, LSQR: an algorithm for sparse linear equations and sparse least squares, *ACM Trans. Math. Software*, **8**, 43–71, 1982.

Parson, T., S. Toda, R. S. Stein, A. Barka, and J. H. Dieterich, Heightened odds of large earthquakes near Istanbul: An interaction-based probability calculation, *Science*, **288**, 661–665, 2000.

Pektaş R., Recent earthquake clusterings in the eastern part of Marmara region and related problems, M. Sc. Thesis, Boğaziçi University, 2001.

Reilinger, R. E., S. C. McClusky, M. B. Oral, R. King, M. N. Toksöz, A. Barka, I. Kinik, O. Lenk, and I. Sanli, Global positioning system measurements of present day crustal movements in the Arabia-Africa-Eurasia Plate Collision Zone, *J. Geophys. Res.*, **102**(B5), 9983–9999, 1997.

Saroğlu, F., O. Emre, and I. Kuscu, Active fault of Turkey. General Directorate of the Mineral Research and Exploration, Ankara, Turkey, 1:2 000 000 scale, 1992.

Seeber, N., J. Armbruster, N. Ozer, M. Aktar, Ş. Bariş, D. Okaya, and Y. Ben-Zion, The 1999 earthquake sequence along the North Anatolian Transform at the juncture between the two main ruptures, and field, in *The 1999 Izmit and Duzce Earthquakes: Preliminary Results*, edited by A. Barka, O. Kozaci, S. Akyuz, and E. Altunel, pp. 209–223, Istanbul Teknik Uni. Yayini, Istanbul, 2000.

Sellami, S., N. Pavoni, D. Mayer-Rosa, S. Mueller, H. Eyidoğan, M. Aktar, C. Gürbüz, Ş. Bariş, O. Polat, and N. Yalcin, Seismicity and seismotectonics of the Bursa Region, in *Active Tectonics of the Northwestern Anatolia—The MARMARA Poly-Project*, edited by C. Schindler and M. Pfister, pp. 449–486, vdf Hochschulverlag AG an der ETH Zurich, 570 pp., 1997.

Şengör, A. M. C., N. Görur, and F. Saroğlu, Strike slip faulting and related basin formation in zones of tectonic escape: Turkey as a case study, *Soc. Econ. Paleont. Min. Spec. Pub.*, **37**, 227–264, 1985.

Smith, A. D., T. Taymaz, F. Oktay, H. Yuce, B. Alpar, H. Basaran, A. J. Jackson, S. Kara, and U. Simsek, High resolution seismic profiling in the Sea of Marmara (NW Turkey): Late Quaternary sedimentation and sea level changes, *GSA Bull.*, **107/8**, 923–936, 1995.

Straub, C. and H. G. Kahle, Global positioning system (GPS) estimates of crustal deformation in the Marmara Sea Region, Northwestern Anatolia, *Earth Planet. Sci. Lett.*, **121**, 495–502, 1994.

Straub, C. and H. G. Kahle, Recent crustal deformation and strain accumulation in the Marmara Sea Region, NW Anatolia, inferred from repeated GPS measurements, in *Active Tectonics of Northwestern Anatolia, The Marmara Poly Project*, edited by C. Schindler, M. Pfister, pp. 417–447,

vdf Hochschulverlag AG an der ETH Zurich, 570 pp., 1997.

Tank, S. B., Y. Honkura, Y. Ogawa, N. Oshiman, M. K. Tunçer, M. Matsushima, C. Çelik, E. Tolak, and A. M. Işikara, Resistivity structure in the western part of the fault rupture zone associated with the 1999 İzmit earthquake and its seismogenic implication, *Earth Planets Space*, **55**, 437–442, 2003.

Taymaz, T., J. Jackson, and D. McKenzi, Active tectonics of the north and central Aegean Sea, *Geophys. J. Int.*, **106**, 433–490, 1991.

Thurber, C. H., Local earthquake tomography: velocities and Vp/Vs—theory, in *Seismic Tomography: Theory and Practice*, edited by H. M. Iyer and K. Hirahara, pp. 563–583, Chapman & Hall, London, 1993.

Toksöz, M. N., A. Shakal, and A. J. Michael, Space-time migration of earthquakes along the North Anatolian Fault Zone and seismic gaps, *Pure Appl. Geophys.*, **117**, 1258–1270, 1979.

Tüncer, M. K., N. Oshiman, Ş. Bariş, Z. Kamaci, M. A. Kaya, A. M. Işikara, and Y. Honkura, Further evidence for anomalous magnetic structure along the active fault in western Turkey, *J. Geomagn. Geoelectr.*, **43**, 937–950, 1991.

Tüncer, M. K., Y. Honkura, N. Oshiman, Y. Ikeda, and A. M. Işikara, Magnetic anomalies related to active folds in the North Anatolian Fault Zone, *J. Geomag. Geoelectr.*, **43**, 813–823, 1991.

Üçer, S. B., S. Crampin, R. Evans, A. Miller, and N. Kafadar, The MAR-NET radio-linked seismometer network spanning the Marmara Sea and the Seismicity of Western Turkey, *Geophys. J. R. Ast. Soc.*, **83**, 17–30, 1985.

Üçer, S. B., H. Eyidoğan, C. Gürbüz, A. Barka, and Ş. Bariş, Seismic investigation of the Marmara region, in *Active Tectonics of Northwestern Anatolia—The MARMARA Poly-Project*, edited by C. Schindler and M. Pfister, pp. 89–100, Hochschulverlag AG an der ETH, Zurich, 500 pp., 1997.

Um, J. and C. Thurber, A fast algorithm for two-point seismic ray tracing, *Bull. Seism. Soc. Am.*, **77**, 972–986, 1987.

Unsworth, M. J., P. A. Bedrosian, M. Esiel, G. D. Egbert, and W. Siripunvaraporn, Along strike variations in the lectrical structure of the San Andreas Fault at Parkfiled, California, *Geophys. Res. Lett.*, **27**, 3021–3024, 2000.

Woith, H., READINESS Project web page, GFZ, Potsdam, Germany, 2003.

Walck, M. C., Three-dimensional Vp/Vs variations for the Coso region, California, *J. Geophy. Res.*, **93**(B3), 2047–2052, 1988.

Yagi, Y. and M. Kikuchi, Source rupture process of the Kocaeli, Turkey, earthquake of August 17, 1999, obtained by joint inversion of near-field data and teleseismic data, *Geophys. Res. Lett.*, **27**, 1969–1972, 2000.

Yaltirak, C., Tectonic evolution of the Marmara Sea and its surroundings, *Mar. Geol.*, **190**, 493–529, 2002.

Yaltirak, C., B. Alpar, M. Sakinc, and H. Yuce, Origin of the Strait of Canakkale (Dardanelles): regional tectonics and the Mediterrenean—Marmara incursion, *Mar. Geol.*, **164**, 139–156, with erratum **167**, 189–190, 2000.

Yilmaz, Y., S. C. Genç, E. Yigitbas, M. Bozcu, and K. Yilmaz, Geological evolution of the late Mesozoic continental margin of Northwestern Anatolia, *Tectonophysics*, **243**, 155–171, 1995.

Young, R. P. and S. C. Maxwell, Seismic characterization of a highly stressed rock mass using tomographic imaging and induced seismicity, *J. Geophys. Res.*, **97**, 12361–12373, 1992.

Zhao, D., A tomographic study of seismic velocity structure in the Japan islans, Ph.D. Thesis, Tohoku Univ., Sendai, Japan, 301 pp., 1991.

Zhao, D. and H. Kanamori, The 1992 Landers earthquake sequence: earthquake occurrence and structural heterogeneities, *Geophys. Res. Let.*, **20**, 1083–1086, 1993.

Zhao, D. and H. Negishi, The 1995 Kobe earthquake: seismic image of the source zone and its implications for the rupture nucleation, *J. Geophys. Res.*, **103**, 9967–9986, 1998.

Zhao, D., A. Hasegawa, and S. Horiuchi, Tomographic imaging of P and S wave velocity structure beneath northeastern Japan, *J. Geophys. Res.*, **97**, 19909–19928, 1992.

Zhao, D., A. Hasegawa, A. Yamamoto, and F. Ochi, Evidence for the location and cause of large crustal earthquakes in Japan, *J. Geophys. Res.*, **105**(B6), 13579–13594, 2000.

Zhao, D., O. P. Mishra, R. Sanda, K. Obara, N. Umino, and A. Hasegawa, Seismological evidence for the influence of fluids and magma on earthquakes, *Bull. Earthq. Res. Inst. Univ. Tokyo*, **76**, 271–289, 2001.

Ş. Bariş, J. Nakajima, A. Hasegawa, Y. Honkura (e-mail: yhonkura@geo.titech.ac.jp), A. Ito, and S. B. Üçer